Symmetries as the Guiding Principle for Flattening Bands of Dirac Fermions

Yarden Sheffer[⬡],[1,*] Raquel Queiroz,[1,2,†] and Ady Stern[1,‡]

[1]*Department of Condensed Matter Physics, Weizmann Institute of Science, Rehovot 7610001, Israel*
[2]*Department of Physics, Columbia University, New York, New York 10027, USA*

Since the discovery of magic-angle twisted bilayer graphene, flat bands in Dirac materials have become a prominent platform for realizing strong correlation effects in electronic systems. Here we show that the symmetry group protecting the Dirac cone in such materials determines whether a Dirac band may be flattened by the tuning of a small number of parameters. We devise a criterion that, given a symmetry group, allows for the calculation of the number of parameters required to make the Dirac velocity vanish. This criterion is employed to study band flattening in twisted bilayer graphene and in surface states of 3D topological insulators. Following this discussion, we identify the symmetries under which the vanishing of the Dirac velocity implies the emergence of perfectly flat bands. Our analysis allows us to construct additional model Hamiltonians that display perfectly flat bands at certain points in the space of parameters: the first is a toy model of two coupled 3D topological insulator surfaces, and the second is a quasicrystalline generalization of the chiral model of twisted bilayer graphene.

I. INTRODUCTION

Since the discovery of superconductivity and correlated insulating states in magic-angle twisted bilayer graphene (TBG) [1–4], moiré materials have drawn tremendous attention as a tunable platform for creating novel electronic effects. The main feature of TBG is that by tuning the twist angle between the graphene layers one can tune the Dirac velocity at the Dirac cones to vanish to a remarkable degree of precision. The vanishing of the Dirac velocity is accompanied by a large density of states (DOS) at charge neutrality, thereby enhancing correlation effects. Following the example of magic-angle TBG, similar fine-tuned systems were shown to exhibit band flattening, with some examples being twisted trilayer graphene [5–8], twisted superconductors [9,10], and moiré patterns on the surfaces of 3D topological insulators (TIs) [11–13].

The emerging plethora of flat-band Hamiltonians in fine-tuned materials raises the question of how generic this phenomenon is. In other words, what characterizes the set of systems for which fine-tuning a small set of parameters leads to the formation of flat bands or almost flat bands?

This question is interesting both from the theoretical and a practical point of view, as a criterion for band flatness should be a useful guide in searching for new materials where exotic correlated phenomena may be found.

In this work, we focus on flat bands in systems harboring Dirac fermions, and more specifically on the conditions for flattening a band by making the Dirac velocity vanish. This scenario is relatively convenient to analyze theoretically, as it requires the knowledge of the Bloch Hamiltonian at only a single k point. The choice to focus on the Dirac velocities can also be motivated by noting that generically an upper bound to the bandwidth may be estimated by a Debye-like approximation to the band dispersion. More rigorously, in many cases of interest (see the examples discussed below) the quadratic order of the band dispersion near the k point vanishes by symmetry. In these cases, the vanishing of the Dirac velocity guarantees that the DOS diverges at least as $(\delta E)^{-1/3}$ near the Dirac point. Note that a quadratic band touching (QBT) cannot be obtained when the Dirac points are fixed by the symmetries of the system (for example, by a rotation symmetry) as a result of the π Berry phase of the Dirac cone [14].

We begin in Sec. II by defining an algebraic criterion: We show that the symmetry group G acting on the Dirac cones determines the number of parameters (e.g., twist angle, pressure, etc.) that should generically be tuned to make the Dirac velocities vanish. This criterion is used to analyze different symmetry groups which can protect a Dirac cone and to find the classes which allow for the tuning of a small number of parameters to obtain vanishing Dirac velocities.

*yarden.sheffer@gmail.com
†raquel.queiroz@columbia.edu
‡adiel.stern@weizmann.ac.il

In Sec. III we apply our criterion to the analysis of two systems of interest. The first one is band flattening of TBG, where we show that the existence of an approximate particle-hole symmetry is necessary for the vanishing of the Dirac velocity. The second system is surface states of 3D TIs under a periodic potential. We show for such systems that the Dirac velocity at charge neutrality can be made to vanish entirely by varying a C_2-symmetric potential. The resulting system might enable a platform for realizing strongly interacting phases on the surface of a TI.

The vanishing of the Dirac velocity may be the first step toward a further increase of the DOS that culminates in a perfectly flat band [15–17]. The first example of a model that exhibits such a band was a toy model of TBG [15]. In Sec. IV we extend the ideas raised by Ref. [17] and our discussion of the vanishing Dirac velocity to discuss the symmetry requirements that are needed to obtain exactly flat bands in general settings. We show that such flat-band Hamiltonians naturally arise in Dirac Hamiltonians with an external SU(2) gauge field by tuning a small number of parameters. For Hamiltonians in class CI of the Altland-Zirnbauer classification [18], we show that the flat-bands condition is equivalent to the vanishing of the Dirac velocity. For Hamiltonians with more general symmetries, we show that the flat bands can be found by considering the vanishing of the velocity in a modified version of the original Hamiltonian, which is in class CI.

We employ our discussion of exactly flat bands in Sec. V where we discuss two new model Hamiltonians which realize such exactly flat bands, along with an in-depth analysis of a recently proposed model. The first example is a continuum model with a C_4 symmetry, which can be thought of as a toy model of two TI surfaces with spin-flipping tunneling and an in-plane position-dependent magnetic field. The second example is a model of a quadratic band-touching Hamiltonian first proposed by [19], on which our analysis can be used to prove analytically the existence of exactly flat bands. The last model is a quasicrystalline generalization of the chiral TBG Hamiltonian. While the latter model does not have well-defined bands, we show it to host "magic angles" with an extensive degeneracy at charge neutrality.

Section VI concludes with a discussion of possible future directions. The appendixes contain a more rigorous definition of our algebraic criterion, reviews of known results published elsewhere, technical proofs, and a discussion of edge cases that are not treated in the main text.

II. CONDITIONS FOR THE VANISHING OF THE DIRAC VELOCITY

A. Zero-velocity codimension

Consider a two-dimensional Bloch Hamiltonian $H(\boldsymbol{k})$ whose band structure has Dirac points for certain values of $\boldsymbol{k}$. The velocity operators at the Dirac points are defined by

$$v_i = \frac{\partial H(\boldsymbol{k})}{\partial k_i}. \tag{1}$$

The Dirac velocities (that is, the dispersion of the Dirac cone close to the Dirac point) are calculated using first-order perturbation theory of $\boldsymbol{v}$ acting on the degenerate wave functions at the Dirac cone. They are the eigenvalues of the matrices

$$\rho(v_i)_{mn} = \langle \psi_m | v_i | \psi_n \rangle, \tag{2}$$

where ψ_m are the degenerate Bloch wave functions at the Dirac cone. We use the notation $\rho(\hat{O})$ to denote the projection of the operator $\hat{O}$ onto the subspace spanned by $\{\psi_m\}$. Most commonly $m = 1, 2$, but we also consider the cases of n_D degenerate Dirac cones, for which $m = 1, \ldots, 2n_D$. We note that when the degenerate Dirac cones are protected by a local unitary symmetry [such as SU(2) spin rotation or a translation symmetry], we can consider each eigenspace of the symmetry separately as a single Dirac cone.

Our main interest is the condition for the Dirac velocities to vanish at some points in the space of parameters. We assume that H is controlled by a set of d parameters $\alpha_1, \ldots, \alpha_d$. We define the *zero-velocity codimension* δ_Z to be the codimension of the manifold in the space of α_i for which $\rho(v_x) = \rho(v_y) = 0$. Roughly speaking, if the Hamiltonian H can have a vanishing Dirac velocity, δ_Z is the number of parameters that should be tuned to make the velocity vanish. Our goal in this section is to show how δ_Z can be calculated from the symmetries that preserve the Dirac cone.

Let G be the group of symmetries that preserve the Dirac cone. For such symmetries $\rho(G)$ is a representation of G, for $g \in G$ being a unitary operator. In the case where g is an antiunitary operator we obtain an antiunitary representation by multiplying the matrix $\rho(g)_{mn}$ by the complex-conjugation operator K. Since the elements g relate states $|\psi_i\rangle$ only to one another, they satisfy

$$\rho(g)\rho(v_i)\rho(g)^{-1} = \rho(gv_ig^{-1}), \tag{3}$$

for all $g \in G$. Note that lattice symmetries can relate v_x and v_y. The tuples $(\rho(v_x), \rho(v_y))$ are therefore elements of the linear subspace V of tuples of $2n_D$-dimensional Hermitian matrices that satisfy Eq. (3). We have

$$\begin{pmatrix} \rho(v_x) \\ \rho(v_y) \end{pmatrix} = \sum_{l=1}^{\delta_Z} f_l(\alpha_1, \ldots, \alpha_d) \begin{pmatrix} M_{l,x} \\ M_{l,y} \end{pmatrix}, \tag{4}$$

where $f_l(\alpha_1, \ldots, \alpha_d)$ are real-valued and $(M_{l,x}, M_{l,y})$ give a basis for V. Consequently, δ_Z is the dimension of V. Equation (4) is then the statement of how the symmetries of the Dirac cones define δ_Z. In the absence of symmetries
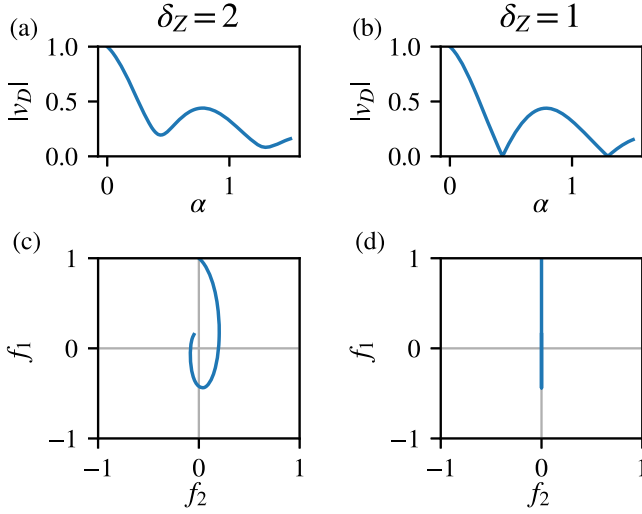
FIG. 1. The trajectory of $\rho(v_x)$ for a varied parameter α. Panels (a) and (c) depict the trajectory of $|v_x|$ and $\rho(v_x)$ [$f_{1,2}$ are defined in Eq. (4)]. Since the trajectory in $f_{1,2}$ does not cross zero the Dirac velocity does not vanish. Panels (b) and (d) are similar but with $\delta_Z = 1$. The additional constraint on $f_{1,2}$ allows $|v_x|$ to vanish on certain values of α.

protecting the Dirac cones, Eq. (4) means trivially that the matrices $\rho(v_i)$ can be expanded in a basis of Hermitian matrices, and δ_Z is the dimension of all possible tuples of such matrices, given by $8n_D^2$ (for example, with $n_D = 1$, M_i could be any of $\sigma_{0,x,y,z}$, giving a total of 8 tuples).

In the case of $\delta_Z = 1$, Eq. (4) reduces to

$$\begin{pmatrix} \rho(v_x) \\ \rho(v_y) \end{pmatrix} = f(\alpha_1, ..., \alpha_n) \begin{pmatrix} M_x \\ M_y \end{pmatrix}. \tag{5}$$

$\rho(v_i)$ are then fixed up to a real parameter and we obtain a vanishing Dirac velocity whenever f vanishes (see Fig. 1). In that case, we can make the Dirac velocity vanish exactly by tuning a single parameter. In Fig. 1 we show the trajectory for $\rho(v_x)$ for $\delta_Z = 2$ and $\delta_Z = 1$ as we vary a single parameter. Noticeably, the Dirac velocity can vanish exactly as α is varied only when $\delta_Z = 1$. In general, given that we have d parameters and δ_Z equations, the dimension of the zero-velocity solutions is $d - \delta_Z$. Note that, since f in Eq. (5) is a continuous function, a change of sign in the Dirac velocity implies the existence of a point where it vanishes. Also, this sign is in agreement with the sign of v_D obtained in perturbation theory, e.g., in Ref. [15].

A slightly more rigorous definition of δ_Z is given in Appendix A. We show there that if the Dirac velocity is made to vanish at some point $\vec{\alpha}_0$ in the parameters space, there exists a manifold of dimension $d - \delta_Z$ around $\vec{\alpha}_0$ in parameter space where the Dirac velocity remains zero. The proof relies on the assumption that the gap between the Dirac point and the rest of the bands does not close. Such closing of the gap results in the Dirac-cone wave functions

not being continuous and can create a boundary to the zero-velocity manifold. We treat an example of such gap closing in Appendix F.

B. Calculation of δ_Z for different symmetry groups

We now follow the principles outlined above to calculate δ_Z for different symmetry groups G which preserve the Dirac point. The symmetry groups we choose to focus on may contain two antiunitary symmetries Θ, Π that anticommute (Θ) and commute (Π), with the operators v_i, as well as their unitary product Σ:

$$\{v_i, \Theta\} = [v_i, \Pi] = \{v_i, \Sigma\} = 0. \tag{6}$$

In cases where the system has local time-reversal T and particle-hole P symmetries that map the Dirac cone onto itself, they may serve as Θ and Π, respectively. Such is the case for a Dirac cone on the surface of a three-dimensional TI. When T, P map between different Dirac cones, such as in the case of TBG, we can combine them with other unitary symmetries to form Θ, Π. We will identify these combinations when we discuss examples of the latter case. In general, we do not demand that the symmetries are local. Furthermore, while we assume that the symmetries either commute or anticommute with the Hamiltonian, we define them only by the commutation relations Eq. (6) and not by their commutation or anticommutation relations with the Hamiltonian.

When the symmetry group G exists, the symmetries constrain the possible representations of the two components of the velocity operator (v_x, v_y). However, as long as the relations Eq. (6) do not distinguish between v_x and v_y, they are not enough to constrain δ_Z to 1, since for any $M_l = (M_x, M_y)$ that satisfies them, $\tilde{M}_l = (M_y, -M_x)$ will do as well, leading to $\delta_Z \geq 2$. To find cases for which $\delta_Z = 1$ we need an additional symmetry that acts differently on v_x and v_y. We therefore consider also a (unitary) reflection symmetry R which takes $x \to -x$ and thus satisfies

$$\{R, v_x\} = [R, v_y] = 0. \tag{7}$$

Our main result in this section is a calculation of δ_Z for all symmetry groups constructed from Θ, Π, Σ, R. Since Θ, Π are antiunitary, different symmetry groups are given by different choices of $\xi_{T,P} = \pm 1$ defined by

$$\Theta^2 = \xi_\Theta.$$
$$\Pi^2 = \xi_\Pi. \tag{8}$$

Besides the sign choice of $\xi_{\Pi,\Sigma}$, different symmetry groups are distinguished by allowing R to either commute or anticommute with Θ, Π, Σ. Namely, for R fixed by $R^2 = +1$ we can choose

TABLE I. δ_Z for the symmetry groups (with Θ, Π, Σ, and/or R symmetries) which preserve a single Dirac cone. Zero indicates the absence of a symmetry, while $\pm$ denote the square of the symmetry. The signs at the subscripts of R indicate whether R commutes or anticommutes with the other symmetries. The calculation of δ_Z here assumes the presence of a C_3 or C_4 symmetry. See Table II for an elaborated calculation of δ_Z. See Ref. [9] for a discussion of the example in row 3, Sec. III A for a discussion of rows 5 and 6, and Sec. III B for discussion of row 7. SC refers to superconductors.

Θ	Π	Σ	R	δ_Z	Example
0	0	0	R	2	
			0	3	
0	0	1	R_-	1	Nodal SC with crystalline symmetries
			0	2	Nodal SC
0	$+$	0	R_+	1	TBG (approximate)
			0	2	TBG (exact), near-commensuration TBG
$-$	$+$	1	R_{-+}	1	$\mathbb{Z}_2$ TI surface states with crystalline symmetries
			0	2	
$-$	0	0	R_-	2	
			0	3	$\mathbb{Z}_2$ TI surface states (general)

$$R\Theta = \zeta_\Theta \Theta R,$$
$$R\Pi = \zeta_\Pi \Pi R,$$
$$R\Sigma = \zeta_\Sigma \Sigma R. \tag{9}$$

Again, $\zeta_{\Theta/\Pi/\Sigma} = \pm 1$ and, assuming that all are present, $\zeta_\Sigma = \zeta_\Theta \zeta_\Pi$. In the case where we have both Θ, Π we use the notation $R_{\zeta_\Theta \zeta_\Pi}$ to denote the commutation or anticommutation relations, while a single subscript is used in the classes where we have only one of Π, Θ, Σ. The resulting family of symmetry groups is similar to that considered in the Altland-Zirnbauer classification with reflection symmetry [18,20–23].

We calculate δ_Z for $n_D = 1, 2$. Table I presents the results for $n_D = 1$. Table II presents the same case with more details and Table III presents the results for $n_D = 2$ (Tables II and III are presented in the Appendixes). The tables are constructed as follows. Assuming that the Dirac cone is n_D-times degenerate, for each symmetry group we construct a representation ρ. We then look for the possible representations of v_x, v_y which satisfy the commutation relations with the symmetry operators obtained from Eqs. (6) and (7). Finally, we assume the presence of a crystalline symmetry relating v_x, v_y such that δ_Z is determined only by the dimension of possible $\rho(v_x)$. Examples of such symmetry are C_3 and C_4 symmetries, where C_n is a rotation of the system by $2\pi/n$.

A similar analysis can be straightforwardly extended to n_D-fold degenerate Dirac cones for higher n_D, include additional symmetries, or extend to three-dimensional Weyl and Dirac nodes [24].

III. APPLICATIONS

A. Magic angles in TBG

As a first application of our analysis, let us consider the band flattening in TBG. Since the two Dirac points are fixed in different k points, we calculate δ_Z for a single Dirac cone. Time reversal T maps between the two valleys of the electronic band. However, when multiplied by C_2, we obtain an antiunitary symmetry that preserves the Dirac point and commutes with the velocity operators, such that it may serve as Π. Furthermore, the C_3 symmetry preserves the Dirac point as well (see a review of the TBG Hamiltonian and symmetries in Appendix B). We fix the representation of these symmetries on the two Dirac point wave functions to be

$$\rho(C_3) = e^{i(2\pi/3)\sigma_z},$$
$$\rho(C_2 T) = \sigma_x K, \tag{10}$$

which is dictated by the requirements that $\rho(C_2 T)$ should be antiunitary, should square to $+1$, and should satisfy $\rho(C_3)\rho(C_2 T)\rho(C_3)^{-1} = \rho(C_2 T)$. For the Dirac cone to be C_3 symmetric we must have $\{v_x, v_y\} = 0$ such that Eq. (4) becomes

$$\rho(v_x) = f_1(\alpha)\sigma_x + f_2(\alpha)\sigma_y,$$
$$\rho(v_y) = f_1(\alpha)\sigma_y - f_2(\alpha)\sigma_x. \tag{11}$$

Evidently, these two symmetries are not sufficient to ensure that the Dirac velocity may be made to vanish with a variation of a single parameter α. Luckily, TBG at small twist angle θ has an additional *approximate* unitary particle-hole symmetry [broken by a term of order $O(\theta)$] given by [25]

$$\mathcal{C}\colon \eta_y \sigma_x K. \tag{12}$$

where η_i are the Pauli matrices acting on the layer indices. This symmetry can be combined with the exact symmetry $C_{2,x}$ to form an additional symmetry that preserves the Dirac cone (see Appendix B for a review of the symmetries of TBG). Thus, under the approximation of a small twist angle the operator $\mathcal{C}C_{2,x}$ maps $x \to -x$ and anticommutes with the Hamiltonian at low energies. Consequently, it commutes with v_x and anticommutes with v_y. Choosing its representation to be σ_x, it fixes $f_2 = 0$. Consequently, the magnitude of the Dirac velocity is given by $|f_1(\alpha)|$, which may be made zero when f_1 changes sign.

This calculation leaves us with an important lesson: in TBG, both the exact and the approximate symmetries are necessary for the Dirac velocity to vanish at the magic angle. Indeed, by diagonalizing the Bistritzer-MacDonald (BM) Hamiltonian [1], we find that when one does not impose the approximate symmetry to be exact, the Dirac
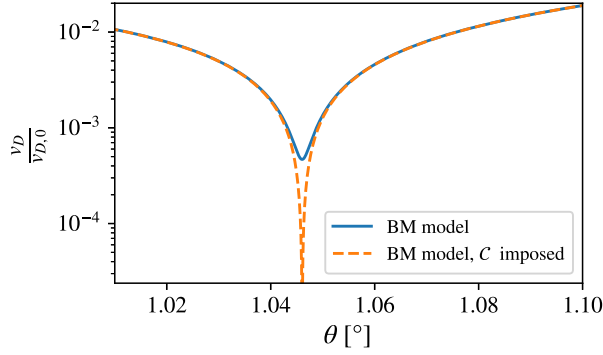
FIG. 2. The Dirac velocity v_D of the BM model [Eq. (B1)], with and without the additional $\mathcal{C}$ symmetry, as the twist angle θ is varied near the magic angle. The $\mathcal{C}$ symmetry is imposed by setting $\theta = 0$ in the $h(\theta)$ terms.

velocity does not reach zero when θ is varied. It instead has a minimum value of $\approx 4 \times 10^{-4} \times v_0$, where v_0 is the Dirac velocity at zero coupling between the layers. The value of v_D as the twist angle is varied, with and without the approximate $\mathcal{C}$ symmetry, is depicted in Fig. 2.

In magic-angle TBG the $\mathcal{C}$ symmetry is weakly broken by a symmetry-breaking term proportional to the small twist angle θ. When the twist angle is not small, for example, when the layers are slightly twisted away from an angle of commensuration [26], the symmetry-breaking term has a non-trivial dependence on the twist angle. In particular, it does not vanish at commensuration angles. In a recent work [26], the authors describe the case of twisted graphene bilayers when the layers are twisted slightly away from a commensurate twist angle. The Hamiltonian obtained is similar to the BM Hamiltonian, but the $\mathcal{C}$ symmetry is broken by a parameter that is independent of the deviation from the commensurate angle. As observed there, the Dirac velocity does not reach zero. Our analysis shows this to be a result of the breaking of $\mathcal{C}$ symmetry.

B. δ_Z in 3D TI surface states

References [11,12] suggested that the velocity characterizing the Dirac cone of the surface of a 3D TI may be suppressed by the application of a periodic potential on the surface. Here we use our analysis of δ_Z to show that there exist "magic parameters" leading to an exact vanishing of the Dirac velocity. We present two types of periodic potentials that lead to a vanishing Dirac velocity. The first possesses a C_4 symmetry and requires tuning a single parameter. The second has only a C_2 symmetry, so that each of v_x, v_y can be made to vanish by tuning a single parameter. The velocity vector can then be made to vanish entirely by tuning two parameters.

The Dirac cone on the surface of a 3D TI is protected by time-reversal symmetry $T = \sigma_y K$. A periodic potential is consistent with this symmetry, leading to the Hamiltonian of the form

$$\mathcal{H} = v_0 \boldsymbol{\sigma} \cdot \boldsymbol{p} + u(\boldsymbol{r}), \tag{13}$$

where v_0 is the Dirac velocity at zero external potential and $u(\boldsymbol{r})$ is a periodic potential term. Note that T allows only for a potential term proportional to the identity in Eq. (13) and prohibits the opening of a gap.

In the case where, in addition to T, there exist additional C_n ($n = 4$, 6) and $M_x = \sigma_y(x \to -x)$ crystalline symmetries [27], we find from Table I that $\delta_Z = 1$ (since the Dirac point maps to itself under time reversal we have $\Theta = T, \Sigma = C_2, R = M_x$).

When a C_2 symmetry is present in the system, $\rho(v_i)$ have no diagonal terms in the basis defined by $|\psi\rangle, T|\psi\rangle$, provided that $|\psi\rangle$ is a Dirac-cone wave function that is a C_2 eigenfunction. The Dirac velocity can then be calculated by

$$v_x = \langle T\psi | v_0 \sigma_x | \psi \rangle = v_0 |\langle K\psi | \sigma_z | \psi \rangle, \tag{14}$$

$$v_y = \langle T\psi | v_0 \sigma_y | \psi \rangle = v_0 \langle K\psi | \psi \rangle. \tag{15}$$

To make the discussion concrete, we start by taking $u(\boldsymbol{r})$ of the form

$$u(\boldsymbol{r}) = 2u_x \cos q_0 x + 2u_y \cos q_0 y. \tag{16}$$

Generally, the Hamiltonian Eq. (13) with Eq. (16) is symmetric under $C_2 = \sigma_z(\boldsymbol{r} \to -\boldsymbol{r})$ and $M_x = \sigma_y(x \to -x)$. When $u_x = u_y$ it is also symmetric under $C_4 = e^{i\pi/4\sigma_z}(\boldsymbol{r} \to \mathcal{R}_4\boldsymbol{r})$. Furthermore, the Hamiltonian anticommutes with the operator:

$$\mathcal{P} = \sigma_z(x \to x + \pi/q_0, y \to y + \pi/q_0). \tag{17}$$

We now analyze the system both in the case where there is an additional C_4 symmetry and where this symmetry is broken.

1. C_4-symmetric case

Our numerical studies of the C_4-symmetric case indicate that the anticommutation of H and $\mathcal{P}$ prevents the vanishing of the Dirac velocity. Indeed, by diagonalizing the Hamiltonian we do not find any magic values (see Fig. 3) as $u = u_x = u_y$ is varied. Besides the calculation presented in the figure, we check that the Dirac velocity does not vanish up to $u = 10$. We also find numerically that the velocity does not vanish even when one considers additional C_4 and $\mathcal{P}$ preserving terms in $u(\boldsymbol{r})$ with higher wave vectors. We therefore conjecture, but cannot prove generally, that a Hamiltonian of the form Eq. (13) with C_4, M_x, and $\mathcal{P}$ symmetries cannot yield a vanishing Dirac velocity for the Dirac cone at charge neutrality.

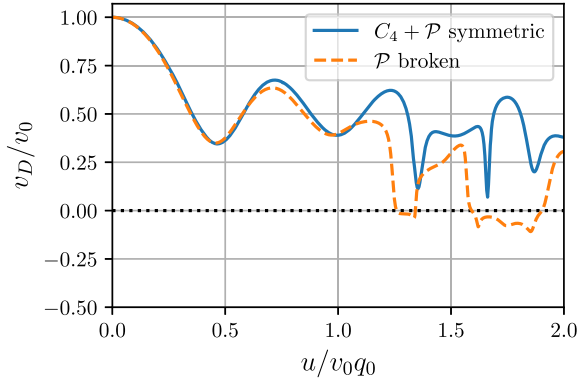One can break $\mathcal{P}$ by introducing higher wave vectors in the potential u. As an example, we take

FIG. 3. The Dirac velocity of the Hamiltonian Eq. (13) with a C_4-symmetric potential in the $\mathcal{P}$-symmetric and $\mathcal{P}$-broken case. The $\mathcal{P}$-symmetric case is defined by the potential Eq. (16) with $u = u_x = u_y$, while the $\mathcal{P}$-broken plot is given for the potential Eq. (17) with $u_1 = u, u_2 = (u/4)$. In the latter case, the velocity is defined as the velocity of the Dirac cone connected adiabatically to the Dirac cone at zero energy as u is increased. One can see that v_x can reach 0 when the $\mathcal{P}$ antisymmetry is broken, but not when it is present.

$$u(\mathbf{r}) = 2u_1(\cos q_0 x + \cos q_0 y)$$
$$+ 2u_2[\cos(q_0 x + q_0 y) + \cos(q_0 x - q_0 y)]. \quad (18)$$

When $\mathcal{P}$ is broken, the Dirac cone, which for $u(\mathbf{r}) = 0$ is at $E = 0$, ceases to be fixed in energy. We can nevertheless calculate the velocity in the Dirac cone connected adiabatically to the one at $E = 0$ as the amplitude of $u(\mathbf{r})$ increases. As an example, in Fig. 3 we plot the Dirac velocity for $u_1 = u, u_2 = u/4$ and find points along the line in which the velocity vanishes. Note that while the first-order dispersion around the Dirac cone vanishes, we still have quadratic terms in the dispersion, leading to a finite (but increased) density of states at the Dirac cone.

In this example, breaking the $\mathcal{P}$ symmetry opens a way for the Dirac velocity to vanish, despite the insensitivity of δ_Z to this breaking. This may indicate that symmetries might also have an impeding role in the tuning of systems parameters to make the Dirac velocity vanish. Indeed, our analysis of δ_Z gives necessary conditions, but not sufficient conditions, for making the Dirac velocity vanish by tuning a given number of parameters.

2. C_4-broken case: Vanishing of the velocity in a single direction

When the periodic potential breaks C_4 symmetry, the difficulties of making the Dirac velocity vanish are alleviated. In this case, each velocity component $v_{x,y}$ vanishes on a codimension-one manifold, which results in $\delta_Z = 2$. Indeed, we find lines of magic parameters u_x, u_y which give one vanishing component of the velocity at charge neutrality (see Fig. 4). By tuning both parameters, we find points at which both components of the velocity vanish.
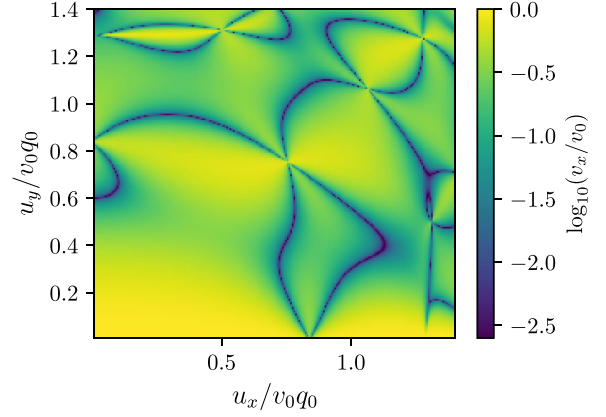

FIG. 4. The x component v_x of the velocity for the Dirac cone at charge neutrality for the Hamiltonian Eqs. (13) and (16) (in logarithmic scale). One sees that v_x vanishes on lines in the u_x, u_y space, giving rise to a low-energy Hamiltonian of the form Eq. (23).

A simple, analytically solvable example of this scenario can be found in the case where $u_y = 0$ and the potential is one dimensional. In that case, we can find zero-energy states of the form

$$\psi_\pm(x) = \sqrt{\frac{q_0}{8\pi}} \begin{pmatrix} e^{iU(x)} \pm e^{-iU(x)} \\ e^{iU(x)} \mp e^{-iU(x)} \end{pmatrix}, \quad (19)$$

$$U(x) = \frac{2u_x}{q_0 v_0} \sin(q_0 x), \quad (20)$$

The Dirac velocities can be obtained from the representations of the velocity operators in this basis. We obtain

$$\rho(v_x) = v_0 \sigma_x, \quad (21)$$

$$\rho(v_y) = v_0 \sigma_y J_0\left(\frac{4u_x}{q_0 v_0}\right), \quad (22)$$

where J_0 is the Bessel function of the first kind. We notice the somewhat surprising result that it is v_x, and not v_y, which is independent of the potential [28], even though the potential varies along the x direction. The matrix $\rho(v_y)$ is proportional to σ_y as a result of the inversion symmetry of $u(x)$ and vanishes on the zeros of J_0. We then find the magic parameters at $u_x/q_0 v_0 = 0.60, 1.38, 2.16, \ldots$.

A velocity that vanishes only in the y direction gives rise to a low-energy Hamiltonian of the form

$$H = \tilde{v}_x \sigma_x k_x + (\tilde{d}_x k_x^2 + \tilde{d}_y k_y^2)k_y \sigma_y, \quad (23)$$

for some parameters $\tilde{v}_x, \tilde{d}_x, \tilde{d}_y$. The DOS resulting from Eq. (23) vanishes as $g(E) \propto E^{1/3}$ at low energies. An interesting question, which is not elaborated on here, is the behavior of the Hamiltonian Eq. (23) when interactions are

also considered. Renormalization-group analysis [29,30] suggests that in the presence of strong enough interactions, the dynamics of the system become quasi-one-dimensional, forming a Luttinger liquid phase in the x direction [31], possibly with spontaneous breaking of translation symmetry in the y direction.

3. C_4-broken case: Vanishing Dirac velocity in both directions, with $\delta_Z = 2$

Since each velocity component vanishes on lines in (u_x, u_y) space, we expect the entire velocity to vanish on points in that space. Figure 5(a) shows that this is indeed the case. In Figs. 5(b) and 5(c), we plot the band structure and DOS at one of these points. One can observe a peak in the DOS at charge neutrality, with two additional peaks corresponding to van Hove singularities (vHS) at nonzero energies. Note that the functional dependency of the two peaks is different: while the DOS at the vHS diverges as $-\log(|\delta E|)$ (with δE being the deviation from the singularity), the DOS diverges as $|\delta E|^{-1/3}$ around charge neutrality. Thus, the points in parameter space where the Dirac velocity vanishes might provide good candidates for strongly interacting states at charge neutrality. Note that the divergence is functionally similar to the higher vHS discussed in Ref. [12], but the low-energy Hamiltonian around the critical point is different [32,33].

The authors of Ref. [11] propose two methods for realizing a Hamiltonian of the form Eq. (16) on the surface of a TI, either by creating a moiré pattern on the surface or by posing a dielectric pattern on it [34]. Here we note that the degree of tunability required to achieve the "magic coupling values" obtained in the C_2-symmetric model can be achieved either by a C_2-symmetric dielectric pattern or by a potential generated by acoustic waves on the surface [35,36]. Note that the dimensionless parameter controlling the coupling strength is $u/q_0 v_0$. Ideally, one would keep both u, q_0 high to mitigate disorder effects and to have a large range of momenta affected by the modulation.

Also, we note that in Ref. [13] the authors show that for two 3D TI surface states a spin-flipping tunneling term allows for the velocity to vanish. When only spin-independent tunneling between two such surfaces is allowed, the surface Hamiltonians can be written in four-component spinors as

$$\mathcal{H}_{\text{twisted TI}} = v_0 \boldsymbol{k} \cdot \boldsymbol{\sigma} + \eta_x u(\boldsymbol{r}) \qquad (24)$$

when η_i are the "surface" indices. The Hamiltonian $\mathcal{H}_{\text{twisted TI}}$, therefore, splits into layer symmetric and antisymmetric sections, each described by the Hamiltonian Eq. (16). Our findings then provide two additional mechanisms for obtaining a Dirac cone with vanishing velocity in such systems.
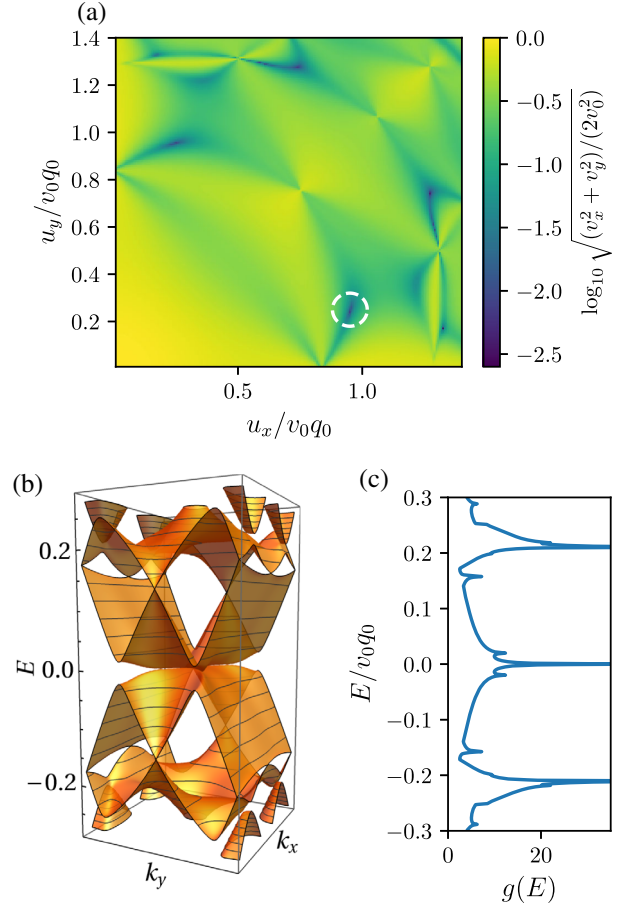

FIG. 5. (a) The "absolute" Dirac velocity $\sqrt{v_x^2 + v_y^2}$ of the Dirac cone at charge neutrality for the Hamiltonian Eqs. (13) and (16) as a function of u_x, u_y, in logarithmic scale. The dark spots are codimension-two manifolds on which the Dirac velocity vanishes entirely. (b),(c) Band structure and DOS of the Hamiltonian Eqs. (13) and (16) at the "magic angle" obtained with $u_x = 0.95$, $u_y = 0.25$ [the point is marked by a circle in (a)]. We find a divergent DOS at charge neutrality with additional van Hove singularities at $E = \pm 0.21$.

IV. EXACTLY FLAT BANDS

An intriguing aspect of the BM Hamiltonian is the presence of a limit [15] in which the Hamiltonian has an additional chiral symmetry and in which the bands at charge neutrality become perfectly flat at the magic angle. These bands may then be chosen to have nonzero Chern numbers and a well-defined sublattice polarization [37]. The Hamiltonian at that limit, referred to as CTBG, allows for exactly flat bands to be reached by tuning a single parameter. In this section, we provide symmetry requirements under which the vanishing of the Dirac velocity implies that the bands are exactly flat. Our analysis provides conditions for small-codimension exactly flat bands.

We begin by considering a generalized form of the CTBG Hamiltonian, described by a Dirac electron in

a background SU(2) gauge field [38]. That is, it is of the form

$$\mathcal{H} = \begin{pmatrix} 0 & \mathcal{D}^\dagger \\ \mathcal{D} & 0 \end{pmatrix},$$
$$\mathcal{D} = 2iv_0(\bar{\partial} + \bar{A}), \qquad (25)$$

where $\bar{\partial} = \frac{1}{2}(\partial_x + i\partial_y)$, $\bar{A} = A_x - iA_y$, with $\vec{A}$ being a non-Abelian traceless gauge potential [here we focus mostly on the SU(2) gauge group]. We assume that $\bar{A}$ is periodic on some lattice. The Hamiltonian $\mathcal{H}$ comes naturally with a chiral symmetry, which we choose to be Hermitian, $S = \sigma_z$. We follow our notation for TBG and use σ_i as the isospin indices and η_i as the gauge indices. For any two solutions $\psi_{a,b}$ of $\mathcal{D}\psi = 0$ (that is, Dirac-cone wave functions in the same S indices) we can define the Wronskian for the functions $\psi_{a,b}$ as

$$\mathcal{I}(\boldsymbol{r}) = \psi_{a,1}(\boldsymbol{r})\psi_{b,2}(\boldsymbol{r}) - \psi_{b,1}(\boldsymbol{r})\psi_{a,2}(\boldsymbol{r}), \qquad (26)$$

where the second index is a spinor index. In Ref. [17] the authors show that $\mathcal{I}(\boldsymbol{r})$ is position independent and further show that the condition for exactly flat bands is the existence of two orthogonal $\psi_{a,b}$ for which $\mathcal{I}(\boldsymbol{r}) = 0$ (see a review in Appendix D). This condition may be expressed as

$$\langle \mathcal{W}\psi_a | \psi_b \rangle = 0, \qquad (27)$$

where $\mathcal{W}$ is the "Wronskian operator" defined by

$$\mathcal{W} = i\eta_y K. \qquad (28)$$

The Wronskian is antiunitary, commutes with S, and satisfies $\mathcal{W}^2 = -1$ (the choice $\mathcal{W} = i\eta_y\sigma_z K$ satisfies the same requirements and gives an equivalent condition). Since the Wronskian inverts the direction of the spinor that it operates on, Eq. (27) implies that

$$\psi_b = \psi_a \nu(\mathbf{r}), \qquad (29)$$

with $\nu(\mathbf{r})$ being a scalar.

Let us consider the symmetry groups which allow a Dirac Hamiltonian as in Eq. (25). We first assume that the symmetries of the system keep $\psi_{a,b}$ orthogonal (this assumption is broken, e.g., in C_3-broken CTBG, which we treat in Appendix E). Since we want the momentum operator to be diagonal in $\mathcal{D}$, it must satisfy the condition

$$v_x v_y = iv_0^2 S. \qquad (30)$$

If the Hamiltonian has additional time-reversal symmetry T, then T and $P = ST$ preserve the space of the two degenerate Dirac cones and therefore satisfy the definition Eq. (6). Using Eqs. (6) and (30) we then find that

$$T, S = 0 \Leftrightarrow T^2 = -P^2. \qquad (31)$$

This requirement already restricts the possible AZ symmetry classes which can support a continuum Hamiltonian with exactly flat bands to AIII (S only), DIII (where $P^2 = -T^2 = 1$), and CI (where $T^2 = -P^2 = 1$). Note that the Hamiltonian Eq. (25) can be thought of as a surface Hamiltonian for class AIII, CI, or DIII topological super-conductors, all of which can have protected Dirac cones on the surface [39,40]. This proves that the Hamiltonian Eq. (25) cannot open a gap at zero energy.

We now treat each one of the above symmetry classes. We first consider the two time-reversal symmetric classes, DIII and CI. We find that class DIII Hamiltonians are too constrained to allow for the condition Eq. (26), while for class CI the condition can be fulfilled and is, in fact, equivalent to the vanishing of the Dirac velocity. We then show that the analysis of class AIII Hamiltonians can be mapped onto the analysis of class CI. Therefore, understanding the criteria for obtaining a flat band in the CI case is sufficient for the more general case of Hamiltonians of the form Eq. (25) with no time-reversal symmetry.

A. Class DIII

Here we prove that a 4×4 Hamiltonian of the form Eq. (25) of class DIII cannot support exactly flat bands. We begin by fixing $v_x = \sigma_x$, $v_y = \sigma_y$, $S = \sigma_z$, and $T = \sigma_y K$ (the choices $T = \eta_x \sigma_y K$ and $T = \eta_z \sigma_y K$, where η are the gauge field indices, are equivalent). This restricts $\bar{A}$ to be of the form

$$\begin{pmatrix} 0 & \bar{A}^\dagger \\ \bar{A} & 0 \end{pmatrix} = a_x(\boldsymbol{r})\sigma_x\eta_y + a_y(\boldsymbol{r})\sigma_y\eta_y \qquad (32)$$

for some real $a_x(\boldsymbol{r}), a_y(\boldsymbol{r})$. Equivalently, we can write

$$\bar{A} = \begin{pmatrix} 0 & -i \\ i & 0 \end{pmatrix} a(\boldsymbol{r}), \qquad (33)$$

where $a(\boldsymbol{r}) = a_x(\boldsymbol{r}) + ia_y(\boldsymbol{r})$. Since $\bar{A}$ commutes with itself at different positions, the equation $\mathcal{D}\psi = 0$ can be straight-forwardly solved by integrating both sides. To do so we decompose $a(\boldsymbol{r})$ as

$$a(\boldsymbol{r}) = \sum_{\boldsymbol{G}} a_{\boldsymbol{G}} e^{(1/2)(z\bar{G}+\bar{z}G)}, \qquad (34)$$

where the sum over $\boldsymbol{G}$ is a sum over reciprocal lattice vectors and $G = G_x + iG_y$. The zero modes of $\mathcal{D}$ can then be calculated explicitly as

$$\psi_\pm(\boldsymbol{r}) = \begin{pmatrix} 1 \\ \pm i \end{pmatrix} f(z)e^{\pm u(\boldsymbol{r})}, \qquad (35)$$

$$u(\boldsymbol{r}) = \sum_{G \neq 0} \frac{2a_{\boldsymbol{G}}}{G} e^{(1/2)(z\bar{G}+\bar{z}G)}$$
$$+ \text{Re}(a_0)(\bar{z} - z) + \text{Im}(a_0)(\bar{z} + z), \qquad (36)$$

where $f(z)$ is holomorphic. Since $e^{\pm u(r)}$ is periodic (up to a phase) and therefore bounded, $\psi_{\pm}$ is normalizable only for $f(z) = \text{const}$. We can conclude that for any $a(r)$ there are only two zero modes for $\mathcal{D}$, which are given by Eq. (35). Since these solutions do not satisfy Eq. (29), there are no exactly flat bands for any choice of $a(r)$. One can explicitly check that the Wronskian $\mathcal{I}(r)$ of ψ_+ and ψ_- is constant and nowhere vanishes, since the spinors are never parallel.

B. Class CI

While class DIII symmetries limit $\bar{A}$ to the form Eq. (33), for class CI $\bar{A}$ does not necessarily commutes with itself at different points. As a result, the zero modes cannot be obtained by an integration procedure similar to Eq. (35). This allows for a richer structure of the zero modes and, most interestingly to us, allows for the vanishing of $\mathcal{I}(r)$.

Further notice that, for class CI Hamiltonians, the combination $v_x T$ satisfies

$$(v_x T)^2 = -v_0^2, \tag{37}$$

$$[v_x T, S] = 0, \tag{38}$$

and thus must be proportional to either $\eta_y K$ or $\sigma_z \eta_y K$. We therefore have

$$\langle \mathcal{W} \psi_a | \psi_b \rangle = \text{const} \times \langle T \psi_a | v_x | \psi_b \rangle. \tag{39}$$

Since the rhs is an element of $\rho(v_x)$, the vanishing of the Dirac velocity implies Eq. (27). This argument shows that in class CI Hamiltonians, as long as the solutions ψ_a and ψ_b are kept orthogonal, the vanishing of the Dirac velocity implies the existence of exactly flat bands. From Table III we see that for class CI (that is, with $\Theta^2 = +1, \Pi^2 = -1$) we have $\delta_Z \leq 2$.

C. Class AIII

For class AIII we can write $\bar{A}$ in the general form:

$$\bar{A}(r) = \begin{pmatrix} W(r) + Z(r) & X(r) + iY(r) \\ X(r) - iY(r) & W(r) - Z(r) \end{pmatrix}. \tag{40}$$

Here W represents the U(1) part of the gauge potential (physically, $\nabla \times W$ is a magnetic field), while X, Y, Z are the three components of the SU(2) part. When $W = 0$ this is a system of class CI with $T = \eta_y \sigma_y K$. Let us first assume for simplicity that $W(r)$ is periodic with mean zero (this represents a staggered magnetic field). We note that, for a zero mode ψ of $\mathcal{D}$, $W(r)$ can be absorbed to ψ by defining

$$\psi'(r) = e^{\bar{\partial}^{-1} W(r)} \psi(r),$$
$$\bar{A}'(r) = \bar{A}(r) - \mathbb{I} \cdot W(r),$$
$$\mathcal{D}' = 2iv_0(\bar{\partial} + \bar{A}'), \tag{41}$$

where the operator $\bar{\partial}^{-1}$ is formally defined by

$$\bar{\partial}^{-1}(e^{-iq \cdot r}) = \frac{2i}{q} e^{-iq \cdot r}, \tag{42}$$

with $q = q_x + iq_y$. Under this definition, we find that $\mathcal{D}\psi = 0$ if and only if $\mathcal{D}'\psi' = 0$. That is, we can reduce the problem of finding a zero mode for $\mathcal{D}$ to the case in which $\bar{A}$ is traceless. We conclude that for finding exactly flat bands of Eq. (25) it is sufficient to solve for the time-reversal symmetric (CI) case, where, as we showed above, the vanishing of the Dirac velocity implies an exactly flat band.

The flat bands created by this procedure have an exact correspondence with lowest-Landau-level (LLL) wave functions [17,41,42], and therefore have a nonzero Chern number for each S polarization (they can, in fact, be written in a form that resembles the LLL wave functions on the plane; see Appendix D). By considering the "squared Hamiltonian" $\bar{H} = \mathcal{H}^2$, for which S acts as a local unitary symmetry, we see that the nonzero Chern number on each S index gives the middle bands a $\mathbb{Z} \times \mathbb{Z}$ topological index when T is absent. This index collapses to a (nonzero) $\mathbb{Z}$ index in the presence of T [43]. Finally, note that CTBG is in class CI, as a result of an emergent intravalley T symmetry [44].

It is important to distinguish between the exactly-flat-bands models discussed here and the flat bands in tight-binding models, e.g., in bipartite lattices [45–48] or in line-graph lattices [49,50]. The models we discuss allow for the creation of exactly flat bands by the tuning of a small number of parameters, assuming that a given set of symmetries is preserved. The small value of the codimension δ_Z implies that even when symmetry-allowed terms give the flat band a dispersion, this dispersion can always be compensated by the lowest-momentum tunneling, and the flatness is recovered. This property is not there in the tight-binding examples. The bipartite lattice models have a flat band in all possible parameters, provided that the lattice remains bipartite. For the line-graph lattices, on the other hand, there is an infinite set of parameters that may be varied to destroy the band flatness while preserving the lattice symmetries, and cannot be compensated by other parameters. A further difference is that the models discussed here are continuum, rather than tight-binding, models. This property allows for the separation of the exactly flat bands to bands of opposite Chern numbers by a symmetry-breaking perturbation, such as a sublattice potential in the case of CTBG. In lattice models, on the other hand, the existence of exactly flat bands with nonzero Chern number is prohibited [51,52] (but such bands may carry fragile topology [48]).

V. EXAMPLES OF CLASS CI FLAT-BAND MODELS

A. Chiral C_4-symmetric model

The insights gained in the previous section can be used to construct a continuum Hamiltonian of class CI that can be

tuned to have exactly flat bands at zero energy. Our model is manifestly distinct from CTBG in that it has a C_4, instead of C_3, symmetry. We therefore call it the C_4-symmetric flat-band model (C4FB). The presence of the C_4 symmetry has additional interesting implications, which will be discussed shortly.

The C4FB model consists of two Dirac cones on two topological insulator surfaces on the x-y plane, connected by z-reflection symmetry, and coupled via a spin-dependent tunneling term modulated by an in-plane magnetic field (a system with slightly similar features was analyzed in Ref. [53]). The two 3D TI surface states are described by [54–57]

$$\mathcal{H}_{\text{TI}} = \eta_z v_0 \boldsymbol{p} \cdot \boldsymbol{\sigma}, \tag{43}$$

where $\boldsymbol{\sigma} = (\sigma_x, \sigma_y)$. Each of these Dirac cones has a chiral symmetry $S = \sigma_z$ and a spinful time-reversal symmetry $T = K\sigma_y$, with $T^2 = -1$. Since we want the system to be in class CI, we need to preserve S and replace T by a symmetry T' satisfying $T'^2 = +1$ and $\{T', S\} = 0$. To that end, we introduce spin-flipping tunneling between the layers, whose phase is modulated by an in-plane magnetic field:

$$\mathcal{H}_{\text{tunneling}} = [\eta_y \cos A_z(\boldsymbol{r}) + \eta_x \sin A_z(\boldsymbol{r})][\boldsymbol{u}(\boldsymbol{r}) \cdot \boldsymbol{\sigma}], \tag{44}$$

where $A_z(\boldsymbol{r})$ is the vector potential associated with the magnetic field. The resulting symmetry $T' = K\eta_x\sigma_x$ is a combination of T and the z reflection $R_z = \sigma_z\eta_x$. The Hamiltonian is then

$$\mathcal{H} = \mathcal{H}_{\text{TI}} + \mathcal{H}_{\text{tunneling}}. \tag{45}$$

We additionally require the symmetries $C_4 = e^{i(\pi/4)\sigma_z}(\boldsymbol{r} \rightarrow \mathcal{R}_4\boldsymbol{r})$, $M_x = \sigma_y(x \rightarrow -x)$ and a translation invariance by the unit cell. While any form of A_z and $\boldsymbol{u}$ satisfying these requirements will give similar results, we choose for concreteness

$$\boldsymbol{u}(\boldsymbol{r}) = u\left(\sin\frac{2\pi x}{a_0}, \sin\frac{2\pi y}{a_0}\right),$$

$$A_z(\boldsymbol{r}) = \phi\left(\cos\frac{2\pi x}{a_0} + \cos\frac{2\pi y}{a_0}\right). \tag{46}$$

Note that $\mathcal{H}$ can be made of the form Eq. (25) by a gauge transformation.

By diagonalizing $\mathcal{H}$ we find that, as expected from our calculation of δ_Z (we have $\Theta = T'$, $\Sigma = S$, $R = M_x$; see Table III), the Dirac velocity vanishes on a codimension-one manifold in the u, ϕ space (see Fig. 6). Our discussion above shows that when the Dirac velocity vanishes, the two degenerate $\sigma_z = +1$ wave functions $\psi_{a,b}$ at $\boldsymbol{k} = 0$
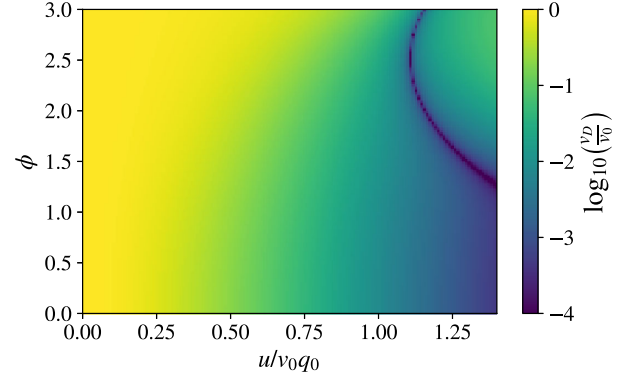

FIG. 6.   Dirac velocity for the Dirac cone of the Hamiltonian Eq. (45) as a function of the parameters u, ϕ, in logarithmic scale. The Dirac velocity vanishes exactly on the dark line, leading to an exact flattening of the bands.

satisfy $\mathcal{I}(\boldsymbol{r}) = 0$. We can therefore write

$$\psi_a(\boldsymbol{r}) = \nu(z)\psi_b(\boldsymbol{r}), \tag{47}$$

where $\bar{\partial}\nu = 0$ since both $\psi_{a,b}$ satisfy $\mathcal{D}\psi = 0$. The function $\nu(z)$ is periodic on the lattice and C_4 symmetric, inherited from $\psi_{a,b}$. Therefore $\nu(z)$ must have at least four poles per unit cell, located at four C_4-related points. At these four points ψ_1 must be zero [58]. Using the fact that ψ_1 has four zeros per unit cell, we can construct four $\sigma_z = +1$ linearly independent zero-energy wave functions at each $\boldsymbol{k}$, in the form [59]

$$\psi_{\boldsymbol{k}}(\boldsymbol{r}) = \Lambda_{\boldsymbol{k},n}(z)\psi_1(\boldsymbol{r}), \tag{48}$$

$$\Lambda_{\boldsymbol{k},n}(z) = e^{ik_x z} \prod_{i=1,\ldots,4} \frac{\vartheta_1\left(\frac{z-w_i}{a_0}\big|i\right)}{\vartheta_1\left(\frac{z-z_i}{a_0}\big|i\right)}, \tag{49}$$

where $\vartheta_1(z|\tau)$ is the Jacobi theta function [60] [we use the convention defined in Eq. (D6)], $z_i = x_i + iy_i$ are the zeros of ψ_1, and w_i satisfy

$$a_0 k = \frac{2\pi}{a_0}\sum_i w_i + n + mi; \qquad m, n \in \mathbb{Z}, \tag{50}$$

where $k = k_x + ik_y$. That is, the positions of w_i determine the momentum of $\psi_{\boldsymbol{k}}$, and the possible configurations of w_i satisfying Eq. (50) give the four degenerate wave functions. This construction is similar to that of lowest-Landau-level wave functions on the torus [61]. Note that our arguments do not rule out the possibility of having more than four wave functions per unit cell, but we expect four to be the general case. We give an example of $\psi_{\boldsymbol{k}=0}$ in Fig. 7.

B. Magic parameters in Hamiltonians with symmetry-protected quadratic band touching

Here we consider a system, previously analyzed in [19], which displays symmetry-protected quadratic band
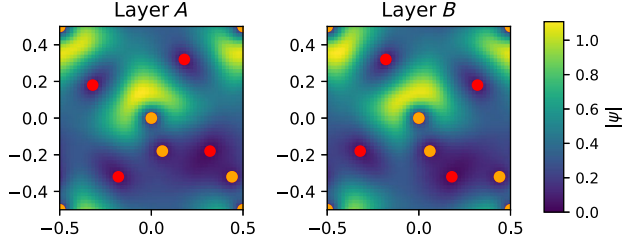
FIG. 7. Example wave function $\psi_{k=0}$ obtained numerically from the Hamiltonian Eq. (45) with $u = 1.1$, $\phi = 2.5$ (at the flat band). Each layer has four mutual zeros, which are zeros of the entire wave function (in orange), and four zeros of opposite chirality which cancel the complex winding of the common zeros (in red).

touching. We show how the symmetry analysis can provide the condition in which a perfectly flat band can be created.

The Hamiltonian we consider is of the form

$$\mathcal{H} = \begin{pmatrix} 0 & \mathcal{D}^*(\boldsymbol{r}) \\ \mathcal{D}(\boldsymbol{r}) & 0 \end{pmatrix}, \tag{51}$$

$$\mathcal{D}(\boldsymbol{r}) = \frac{1}{2m_0}\bar{\partial}^2 + u(\boldsymbol{r}), \tag{52}$$

where $u = u_x + iu_y$. In Ref. [19], the authors suggest realizing this Hamiltonian by stacking two twisted layers of a material hosting a QBT point at the K points. The Hamiltonian shown there realizes two copies of $\mathcal{H}$ with

$$u(\boldsymbol{r}) = u_x(\boldsymbol{r}) = \alpha(\cos qx - \cos qy). \tag{53}$$

Below we provide a proof that $\mathcal{H}$ with $u(\boldsymbol{r})$ given by Eq. (53) has flat bands with codimension one in α (this was shown numerically in Ref. [19]).

1. From a QBT to a Dirac Hamiltonian

As a first step, we show the relation between $\mathcal{H}$ and the Hamiltonians discussed in Sec. IV. We first note that $\mathcal{H}$ has a time-reversal symmetry $\mathcal{T} = \sigma_x K$ and a chiral symmetry $\mathcal{S} = \sigma_z$, and is therefore in class CI, just as the flat-bands Hamiltonian discussed there. Furthermore, we can relate the two-band Hamiltonian Eq. (51), which has second-derivative operators, to a four-band class CI Hamiltonian of the form Eq. (25) having only first-derivative operators, and having the same number of zero-energy states.

To do so, we notice that for any scalar wave function ψ satisfying $\mathcal{D}\psi = 0$, we have

$$\tilde{\mathcal{D}} \begin{pmatrix} \psi \\ v_0\bar{\partial}\psi \end{pmatrix} = 0, \tag{54}$$

where

$$\tilde{\mathcal{D}} = \begin{pmatrix} v_0\bar{\partial} & -1 \\ u & v_0\bar{\partial} \end{pmatrix}, \tag{55}$$

and $v_0 = (2m_0)^{-1/2}$. As a result, the four-component spinor $(0, 0, \psi, v_0\bar{\partial}\psi)$ is a zero-energy state of the Hamiltonian

$$\tilde{\mathcal{H}} = \begin{pmatrix} 0 & \tilde{\mathcal{D}}^\dagger \\ \tilde{\mathcal{D}} & 0 \end{pmatrix}. \tag{56}$$

Notably, $\tilde{\mathcal{H}}$ inherits the class CI symmetries of $\mathcal{H}$, which are given by $\tilde{\mathcal{T}} = \eta_y\sigma_y K$, $\tilde{\mathcal{S}} = \sigma_z$ (σ_i, η_i are the Pauli matrices in the spinor and gauge components, respectively). Similarly, it inherits any crystalline symmetry that $\mathcal{H}$ has. This shows that finding conditions for a flat band in Hamiltonians of the form Eq. (51) is equivalent to finding the conditions for a flat band in class CI Dirac Hamiltonians, which were analyzed in Sec. IV. There we showed that a flat band will be created as a result of a vanishing Dirac velocity, provided that $\tilde{\mathcal{D}}$ has two orthogonal zero modes. We notice that here, for $u = 0$, $\tilde{\mathcal{H}}$ has a QBT, which amounts to having a vanishing Dirac velocity [i.e., a vanishing expectation of the operator Eq. (1)] with only a single zero mode of $\tilde{\mathcal{D}}$. To conclude our argument, we show that when the quadratic term in the dispersion is made to vanish by the application of u, the QBT can be separated into two Dirac cones with vanishing velocity, resulting in perfectly flat bands.

2. From a Dirac Hamiltonian to a perfectly flat band

We now apply our analysis to provide conditions for the emergence of exactly flat bands in $\mathcal{H}$. We first notice that the QBT is stable when u is modified if and only if $\tilde{\mathcal{H}}$ is C_4 symmetric. When the QBT is unstable we get a similar situation to the one discussed in Appendix E: the model has two zero-energy Dirac points, whose momenta change as u is modified. As a result, the vanishing of the Dirac velocity will result in the Dirac points fusing to a QBT with nonzero quadratic dispersion, and exactly flat bands will not generally form. To go on further we, therefore, need to assume that $\mathcal{H}$ is C_4 symmetric with $C_4 = \sigma_z(x \to y, y \to -x)$ (which is also the case for the model discussed in Ref. [19]).

With the assumption of a C_4 symmetry, we investigate which additional symmetries can help us make the bands perfectly flat. The form of $\tilde{\mathcal{H}}$ ensures that the dispersion remains quadratic around the band-touching point, so the projected Hamiltonian near the K point is restricted to the form

$$\tilde{\mathcal{H}}_{\text{proj}}(\boldsymbol{k}) = \begin{pmatrix} 0 & [f_1(\alpha) + if_2(\alpha)]k^2 \\ [f_1(\alpha) - if_2(\alpha)]\bar{k}^2 & 0 \end{pmatrix}$$
$$+ O(k^4). \tag{57}$$

Consequently, the quadratic dispersion of $\tilde{\mathcal{H}}$ vanishes with codimension two. To reduce the codimension to one we require an additional symmetry that guarantees the vanishing of f_2, which is a reflection symmetry. Acting on $\mathcal{H}$, this additional symmetry is equivalent to the requirement that u is either purely real or purely imaginary.

Having shown that the quadratic term in the dispersion can be made to vanish, we now show that this vanishing leads to perfectly flat bands. To do so, we map the problem to the problem studied previously, where we had two separate zero modes $\psi_{a,b}$ of $\tilde{\mathcal{D}}$. This can be done by adding a small C_4-breaking perturbation to u, of the form

$$u \to u - v_r(\alpha)k_\varepsilon, \tag{58}$$

where $v_r(\alpha) = \sqrt{f_1(\alpha) + if_2(\alpha)}$ is the square root of the renormalized quadratic dispersion around the K point and k_ε is small. The resulting Hamiltonian has, therefore, two Dirac points at $\boldsymbol{k} = (\pm k_\varepsilon, 0)$, which remain separate for any α. In addition, the Dirac velocity of the Dirac cones vanishes whenever α is tuned to make v_r vanish. From the analysis of Sec. IV, we conclude that $\tilde{\mathcal{H}}$ with the additional perturbation has exactly flat bands whenever v_r vanishes and, taking k_ε to zero, we conclude that $\tilde{\mathcal{H}}$ and therefore $\mathcal{H}$ have exactly flat bands whenever v_r vanishes.

The analysis in this section shows, therefore, that Hamiltonians of the form Eq. (51) with a C_4 symmetry have exactly flat bands with a small codimension (one if there is a reflection symmetry present and two otherwise). We note that, while an example of such a Hamiltonian was first provided in Ref. [19] using two twisted layers of a 2D material with QBT points, the u term in Eq. (51) can be obtained by a long-wavelength modification of the hopping in a single layer hosting a QBT point (for example, by periodic strain from surface-acoustic waves).

C. Quasicrystalline generalization of CTBG

Here we discuss a quasicrystalline generalization of the CTBG Hamiltonian, namely, the generalization of the C_3-symmetric model to a C_n-symmetric model for odd $n \geq 3$. We focus on the chiral case as it is the easiest to analyze theoretically. The family of Hamiltonians is given by the form Eq. (25) with

$$\bar{A} = \begin{pmatrix} 0 & \frac{\alpha}{2}U(\boldsymbol{r}) \\ \frac{\alpha}{2}U(-\boldsymbol{r}) & 0 \end{pmatrix},$$

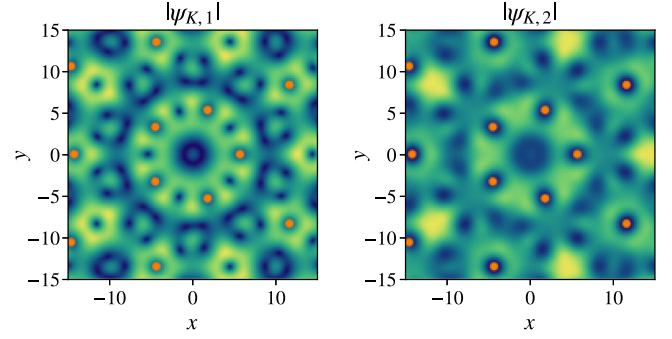$$U(\boldsymbol{r}) = \sum_{j=0}^{n-1} e^{i(2\pi/n)j} e^{-i\boldsymbol{q}_i \cdot \boldsymbol{r}}, \tag{59}$$

FIG. 8. The wave function ψ_K in the chiral C_5-symmetric model Eq. (59) at the magic angle. The orange points signify zeros of the wave function.

with $\boldsymbol{q}_j = [\cos(2\pi j/n - \pi/2)], \sin[2\pi j/n - \pi/2)]$. Clearly, Eq. (59) reduces to the CTBG Hamiltonian [15] for $n = 3$. For $n > 3$ the model is not crystalline anymore, but nevertheless the formal analysis of magic angles in CTBG continues to hold. That is, we can calculate by perturbation theory in α the correction to the zero-energy wave functions. We get a zero-energy wave function of the form

$$\psi_K(\boldsymbol{r}) = \sum_{n=0}^{\infty} (\alpha \bar{\partial}^{-1} \bar{A})^n \begin{pmatrix} 1 \\ 0 \end{pmatrix}, \tag{60}$$

where the operator $\bar{\partial}^{-1}$ is defined in Eq. (42). Note that $\bar{\partial}^{-1}$ is undefined for $\boldsymbol{q} = 0$, but the C_n symmetry prevents zero-momentum terms from appearing in the perturbation series. Another zero-energy wave function is given by acting on ψ_K with the intravalley C_2 symmetry $C_2 = \eta_y(\boldsymbol{r} \to -\boldsymbol{r})$.

While the Dirac velocity is no longer well defined (as there are no Bloch wave functions), the Wronskian operator $\mathcal{W}$ given by Eq. (28) still is. Since the "Dirac cone" wave functions are still reflection symmetric, we have $\delta_Z = 1$ for the vanishing of the formal Dirac velocity given by

$$v_D = \langle C_2\psi_K | \mathcal{W} | \psi_K \rangle = \langle \psi_K(-\boldsymbol{r}) | \psi_K(\boldsymbol{r}) \rangle. \tag{61}$$

When v_D vanishes we find from Eq. (D4) that ψ_K must have extensively many zeros (that is, the number of zeros in a given area being proportional to the area). By repeating the analysis in Appendix D we, therefore, find a "band" with an extensive degeneracy of zero-energy wave functions.

In Appendix G we describe the results of a perturbative calculation of v_D similar to the one detailed in Ref. [15]. For $n = 5$ we find the first magic angle at $\alpha_0 = 0.32$. We plot the resulting wave function in Fig. 8. Each zero of the wave function can be used to construct a zero-energy state. If the system is confined to a finite size L, the number of zero-energy states (up to corrections of order $1/L$) will equal the total number of zeros of the magic-angle wave function, and will be extensive with the system size.

VI. DISCUSSION

In this work, we discuss the symmetry structure that is required for the flattening of bands of Dirac fermions. We start with the requirement for the Dirac velocity to vanish and give examples in TBG and a Dirac cone on the surface of a 3D topological insulator. Afterward, we discuss the vanishing of any dispersion, namely, the symmetry requirements for the formation of exactly flat bands. We show that, for a certain set of symmetries, the vanishing of the Dirac velocity implies that the band is exactly flat.

The symmetry considerations which allow us to calculate δ_Z do not provide us with a recipe for writing a Hamiltonian with δ_Z parameters which can have a vanishing velocity, but generically suggest natural candidates for flat-band Hamiltonians. In one of the cases, which we studied in Sec. III, the existence of an extra symmetry seems to impede such vanishing by the most natural candidate Hamiltonian. This observation may indicate that there may be further symmetry considerations that may guide the search for such Hamiltonians. These are left here as a subject for future research.

While in this work we focus mainly on 2D moiré materials, much of our discussion can be straightforwardly extended to other systems and different tuning parameters. For example, one can consider 3D nodal line materials, where each k_z slice can be viewed as a 2D subsystem, and k_z can serve as an adiabatic parameter. Another interesting future question is the generalization of our results in Sec. IV to the case of $SU(N)$ gauge fields. Studies of specific models, such as alternating-twist n-layer graphene [5] and chiral twisted graphene multilayers [62,63], show the richness of states that might arise in such cases. In the former, one can encounter exactly flat bands coexisting with dispersive bands, while in the latter we see exactly flat bands with Chren numbers $C > 2$. It would be interesting to see whether it is possible to give a classification of the possible states in that case, in terms of the underlying symmetries.

Finally, another interesting direction is an experimental realization of the models we present here. The flat-band models discussed in Sec. V are theoretically intriguing, but more work is needed if one wishes to find candidates for experimental systems which host them. On the other hand, we believe that the TI models discussed in Sec. III can be realized using currently available experimental capabilities. Such an increase in the density of states on the surface of a TI could give rise to intrinsic superconductivity or correlated insulators [64] on the surface of a TI, or, more exotically, a gapped state that is symmetric to both time reversal and charge conservation. Such a state must be topologically ordered with quasiparticles satisfying non-Abelian statistics [65–70].

ACKNOWLEDGMENTS

APPENDIX A: RIGOROUS DEFINITION OF δ_Z

Here we provide a more rigorous notion of δ_Z. Specifically, we prove the following theorem.

Theorem.—Let $H_{\vec{a}}(\boldsymbol{k})$ be a Bloch Hamiltonian with n_D degenerate Dirac cones at $\boldsymbol{k} = \boldsymbol{k}_D$ with energy E_D (in general, both k_D and E_D can depend on $\vec{\alpha}$), such that $H_{\vec{a}}(\boldsymbol{k}_D)$ is symmetric under a group G. We assume that $H_{\vec{a}}$ is controlled by a set of continuous parameters $\vec{\alpha} = \alpha_1, \ldots, \alpha_d$ such that the Dirac point has the same degeneracy for all values of $\vec{\alpha}$. Further assume that for some parameter choice $\vec{\alpha}_0$ the Dirac velocity matrices,

$$\rho(v_i)_{mn} = \langle \psi_m | v_i | \psi_n \rangle, \tag{A1}$$

vanish and that the gap between the degenerate Dirac cone wave functions and the higher bands is not closed. Then there exists (locally) a manifold of dimension $\geq d - \delta_Z$ in $\vec{\alpha}$ space in which Eq. (A1) vanishes. Here $\delta_Z > 0$ is defined by Eq. (4) as the dimension of the vector space V of tuple of matrices (M_x, M_y) satisfying Eq. (3).

Before proving the theorem, a few notes are in order.

(1) The symmetries in G can be either unitary or antiunitary. We also allow for symmetries that anticommute with $H(\boldsymbol{k}_D)$.

(2) Here δ_Z is an *upper bound* to the codimension of the zero-velocity manifold. Cases where δ_Z is strictly larger than the codimension should arise in the case where there are additional low-energy emergent symmetries at the Dirac cones. An example can be given in the C_3-broken CTBG Hamiltonian [Eq. (E1)]: In this case, the exact Hamiltonian does not have a rotational symmetry relating v_x and v_y. On the other hand, the velocity operators satisfy Eq. (30), giving rise to an additional constraint on the codimension.

(3) When the gap with the upper bands closes, the Dirac velocity representations are no longer required to be continuous since ψ_i are no longer continuous. A gap closing can therefore create a boundary (of dimension $< d - \delta_Z$) to the zero-velocity manifold. We give an example of this scenario in Appendix F.

Proof.—Since the gap between the degenerate point and the other bands does not close, we can calculate the correction to $\rho(\hat{o})$ for any operator $\hat{o}$ via first-order

perturbation theory; that is,

$$\frac{\partial\rho(\hat{o})_{mn}}{\partial\vec{\alpha}} = \left\langle\frac{\partial\psi_m}{\partial\vec{\alpha}}|\hat{o}|\psi_n\right\rangle + \left\langle\psi_m|\frac{\partial\hat{o}}{\partial\vec{\alpha}}|\psi_n\right\rangle$$
$$+ \left\langle\psi_m|\hat{o}|\frac{\partial\psi_n}{\partial\vec{\alpha}}\right\rangle, \quad (A2)$$

where for the velocity operator,

$$\frac{\partial\psi_n}{\partial\vec{a}} = \sum_i{}' \frac{\langle\psi_i|\frac{\partial H}{\partial\vec{\alpha}}|\psi_n\rangle}{E_i - E_n}|\psi_i\rangle, \quad (A3)$$

$$\frac{\partial\hat{o}}{\partial\vec{\alpha}} = \frac{\partial^2 H}{\partial\vec{\alpha}\partial k_i}, \quad (A4)$$

with the sum running only on ψ_i outside the degenerate space. In the case of unitary operators $g \in G$, which preserve the degenerate subspace, we have

$$\left\langle\psi_m|g|\frac{\partial\psi_n}{\partial\vec{\alpha}}\right\rangle = 0, \quad (A5)$$

$$\frac{\partial g}{\partial\vec{\alpha}} = 0, \quad (A6)$$

so we find $\partial_{\vec{\alpha}}\rho(g) = 0$. We then get for v_i that

$$\rho(g)^{-1}\frac{\partial\rho(v_i)}{\partial\vec{\alpha}}\rho(g) = \frac{\partial}{\partial\vec{\alpha}}[\rho(g)^{-1}\rho(v_i)\rho(g)]$$
$$= \frac{\partial}{\partial\vec{\alpha}}\rho(g^{-1}v_i g). \quad (A7)$$

We also have

$$g^{-1}v_i g = \sum_j \gamma_{i,j}^g v_j, \quad (A8)$$

where $\gamma_{i,j}^g$ are real constants that depend on whether g commutes or anticommutes with H, as well as the transformation that g induces on k. Combining Eqs. (A7) and (A8) gives

$$\rho(g)^{-1}\frac{\partial\rho(v_i)}{\partial\vec{\alpha}}\rho(g) = \sum_j \gamma_{i,j}^g \frac{\partial\rho(v_j)}{\partial\vec{\alpha}}. \quad (A9)$$

For a given set of matrix representations $\rho(g)$ for $g \in G$, Eq. (A9) gives a set of linear equations on the tuples $(\rho(v_x), \rho(v_y))$. The tuples satisfying Eq. (A9) then form a vector space whose dimension is δ_Z [see the definition of δ_Z in Eq. (4)]. There must therefore be at least $d - \delta_Z$ directions in $\vec{\alpha}$ space in which the velocity does not change, giving a (local) zero-velocity manifold around $\vec{\alpha}_0$ whose dimension is at least $d - \delta_Z$. ∎

APPENDIX B: REVIEW OF THE BISTRITZER-MACDONALD MODEL AND SYMMETRIES

Here we review the continuum model of twisted bilayer graphene proposed by Bistritzer and MacDonald [1].

1. TBG Hamiltonian

The Bistritzer-MacDonald Hamiltonian describes twisted bilayer graphene at small angles and low energies, at a single valley of the graphene layers. It is given by [1,71,72]

$$H = \begin{pmatrix} h(-\theta/2) & T(\mathbf{r}) \\ T^\dagger(\mathbf{r}) & h(\theta/2) \end{pmatrix}, \quad (B1)$$

$$h(\theta) = -iv\boldsymbol{\sigma}_\theta \cdot \boldsymbol{\nabla}, \quad (B2)$$

$$T(\mathbf{r}) = w\sum_j e^{-i\mathbf{q}_j\cdot\mathbf{r}}T_j, \quad (B3)$$

where $\boldsymbol{\sigma}_\theta = e^{-i\theta\sigma_z/2}(\sigma_x, \sigma_y)e^{i\theta\sigma_z/2}$. The single-layer h are the Hamiltonians for a single Dirac cone in each graphene layer, twisted by a small angle. The tunneling matrices T_i are

$$T_1 = \begin{pmatrix} \kappa & 1 \\ 1 & \kappa \end{pmatrix},$$
$$T_{2,3} = \begin{pmatrix} \kappa & e^{\mp i\phi} \\ e^{\pm i\phi} & \kappa \end{pmatrix}, \quad (B4)$$

with $\phi = 2\pi/3$ and $\mathbf{q}_1 = k_\theta(0, -1)$, $\mathbf{q}_{2,3} = k_\theta(\pm\sqrt{3}, 1)/2$. We have $k_\theta = 2\sin(\theta/2)k_D \approx \theta k_D$, where $k_D = (4\pi/3\sqrt{3}a_0)$ and $a_0 \approx 1.4$ Å is the distance between atoms in graphene. The scale $w \approx 110$ meV is the energy scale associated with the tunneling between the layers, and the factor $0 \le \kappa \le 1$ determines the ratio between AA and AB tunneling between the sublattices of the graphene layers. Real-world TBG has $\kappa \approx 0.7$ as a result of lattice relaxation [73].

Important to some of our discussion is the chiral limit of TBG (CTBG) obtained by setting $\kappa = 0$. Under this assumption, we can remove the θ dependence in $h(\theta/2)$ by a gauge transformation. To write the resulting Hamiltonian in a form compatible with Eq. (25), we further rescale the Hamiltonian by defining $\mathcal{H} = H/E_0$, where $E_0 = k_\theta w$, define the dimensionless parameter $\alpha = w/k_\theta v$, and rearrange the rows so that the Hamiltonian acts on the spinor $(\psi_1, \psi_2, \chi_1, \chi_2)$ (here the indices are layer indices, and ψ, χ live on the A, B sublattices, respectively). We obtain the chiral Hamiltonian [15,38]

$$\mathcal{H}_{\text{chiral}} = \begin{pmatrix} 0 & \mathcal{D}^*(-\mathbf{r}) \\ \mathcal{D}(\mathbf{r}) & 0 \end{pmatrix},$$
$$\mathcal{D}(\mathbf{r}) = \begin{pmatrix} -2ik_\theta^{-1}\bar{\partial} & \alpha U(\mathbf{r}) \\ \alpha U(-\mathbf{r}) & -2ik_\theta^{-1}\bar{\partial} \end{pmatrix}, \quad (B5)$$

where $z = x + iy$, $\bar{\partial} = \frac{1}{2}(\partial_x + i\partial_y)$, and $U(\mathbf{r}) = e^{i\mathbf{q}_1 \cdot \mathbf{r}} + e^{i\phi}e^{-i\mathbf{q}_2 \cdot \mathbf{r}} + e^{-i\phi}e^{-i\mathbf{q}_2 \cdot \mathbf{r}}$.

2. Symmetries

Let us discuss the symmetries of the BM Hamiltonian Eq. (B1). We define the Pauli matrices σ_i, η_i in sublattice and layer space, respectively. The point symmetries acting within the valley are given by [74]

$$C_2T:\ \sigma_x K(\mathbf{r} \to -\mathbf{r}),$$
$$C_3:\ e^{-i(2\pi/3)\sigma_z}(\mathbf{r} \to R_3\mathbf{r}),$$
$$C_{2,x}:\ \eta_x\sigma_x(y \to -y), \qquad (B6)$$

where K is the complex-conjugation operator and R_3 is the rotation matrix by $2\pi/3$. Of the three symmetries described above, only the first two preserve the Dirac points.

As a result of the small angle between the layers, the BM Hamiltonian has an additional approximate particle-hole symmetry. If we take the approximation of setting $\theta = 0$ in $h(\theta)$, the resulting Hamiltonian has a particle-hole symmetry given by [25]

$$\mathcal{C}:\ \eta_y\sigma_x K. \qquad (B7)$$

In the real-world model of TBG, the symmetry is broken in order $\mathcal{O}(\theta)$. The combination $\mathcal{C}C_{2,x}$ gives an additional antisymmetry that preserves the Dirac cone; that is,

$$\mathcal{C}C_{2,x}:\ \eta_z K(y \to -y). \qquad (B8)$$

Finally, the chiral model has, besides $\mathcal{C}$, the additional chiral symmetry

$$S:\ \sigma_z. \qquad (B9)$$

Since in the chiral model the θ dependence in h is removed by a gauge transformation, the unitary particle-hole symmetry $\mathcal{C}$ is exact here. We can therefore combine S and $\mathcal{C}$ to obtain an intravalley unitary rotation symmetry that sends $\mathbf{r} \to -\mathbf{r}$ [44]. By combining the intravalley rotation with C_2T we obtain the intravalley time-reversal symmetry $T' = \sigma_y\eta_y K$ which satisfies $(T')^2 = +1$. This shows that the CTBG model is indeed in class CI.

APPENDIX C: ADDITIONAL PARAMETERS FOR TUNING A C_2-SYMMETRIC VANISHING-VELOCITY DIRAC CONE

Here we elaborate on our discussion of the Dirac cone on the surface of a 3D TI. In particular, we study additional parameters (besides the potential amplitude) which can be tuned to obtain a vanishing velocity for a C_2-symmetric Dirac cone in a potential. The Hamiltonian of the form
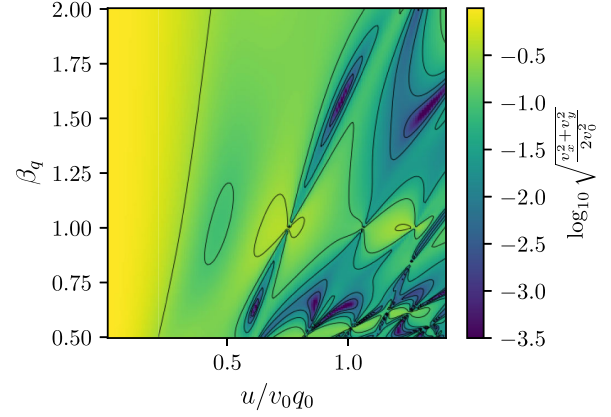

FIG. 9. The "absolute Dirac velocity" of the Dirac cone at charge neutrality of the Hamiltonian Eq. (C2) [similar to Fig 5(a)]. The dark valleys are points of vanishing velocity.

Eqs. (13) and (16) is defined to be consistent with the T, M_x, and C_2 symmetries, but is not the most general form consistent with these symmetries. More generally, we can write an anisotropic form for the Dirac cone:

$$\mathcal{H} = v_x\sigma_x p_x + v_y\sigma_y p_y + 2u_x\cos q_x x + 2u_y\cos q_y y. \qquad (C1)$$

Here v_x/v_y can be controlled by applying strain on the TI while q_x/q_y can be controlled (for example) by an asymmetry in the dielectric pattern. By rescaling the y axis we can make $v_y = v_x = v_0$. We, therefore, write the Hamiltonian

$$\mathcal{H} = v_0\mathbf{p}\cdot\boldsymbol{\sigma} + 2u(\cos q_0 x + \beta_u\cos q_0\beta_q y), \qquad (C2)$$

which is controlled by the dimensionless parameters $\beta_u, \beta_q, u/q_0 v_0$ (the first two define the C_4-symmetry breaking). In Fig. 9 we plot the velocity of the Dirac cone of Eq. (C2) at charge neutrality as a function of u, β_q. The results show similar magic parameters to the case discussed in the main text [see Fig. 5(a)].

APPENDIX D: WRONSKIAN OPERATOR AND REQUIREMENTS FOR EXACTLY FLAT BANDS

In this appendix, we restate some results from Ref. [17] that are useful to our discussion of the condition of exactly flat bands in chiral-symmetric continuum models. We begin with a Hamiltonian of the form

$$\mathcal{H} = \begin{pmatrix} 0 & \mathcal{D}^\dagger \\ \mathcal{D} & 0 \end{pmatrix},$$
$$\mathcal{D} = -2iv_0(\bar{\partial} + \bar{A}), \qquad (D1)$$

where $\bar{\partial} = \frac{1}{2}(\partial_x + i\partial_y)$, $\bar{A} = A_x - iA_y$, with $\vec{A}$ being an SU(2) gauge potential. We assume that $\mathcal{H}$ is symmetric under translations by the lattice vectors $\mathbf{a}_1$, $\mathbf{a}_2$. Given two

solutions ψ_a, ψ_b of the zero mode equation,

$$\mathcal{D}\psi(\mathbf{r}) = 0, \qquad (\text{D2})$$

one can write the Wronskian:

$$\mathcal{I}(\mathbf{r}) = \psi_{a,1}(\mathbf{r})\psi_{b,2}(\mathbf{r}) - \psi_{b,1}(\mathbf{r})\psi_{a,2}(\mathbf{r}). \qquad (\text{D3})$$

Importantly, we find that $\mathcal{I}(\mathbf{r}) = $ const. This is because

$$\bar{\partial}\mathcal{I}(\mathbf{r}) = i\bar{\partial}(\psi_a^T \eta_y \psi_b) = -i\psi_a^T(\bar{A}^T\eta_y + \eta_y\bar{A})\psi_b$$
$$= -i\psi_a^T(\eta_y \operatorname{tr}\bar{A})\psi_b = -\operatorname{tr}\bar{A} \cdot \mathcal{I}(\mathbf{r}).$$

When there is no external magnetic field, we have $\operatorname{tr}\bar{A} = 0$, so $\mathcal{I}(\mathbf{r}) = \mathcal{I}(z)$. However, since $\mathcal{I}(z)$ has no singularity it must be constant.

Next, we find that when $\mathcal{I} = 0$, there must be an exactly flat band at zero energy. This is because, in that case, we must have

$$\psi_b(\mathbf{r}) = \nu(\mathbf{r})\psi_a(\mathbf{r}). \qquad (\text{D4})$$

We have, however, $\bar{\partial}\nu(\mathbf{r}) = 0$, as can be seen by applying $\mathcal{D}$ on both sides of Eq. (D4). We can therefore write $\nu(\mathbf{r}) = \nu(z)$. Assuming that $\psi_{a,b}$ are orthogonal (which must be the case if they are positioned on different points in the BZ), $\nu(z)$ is a nonconstant meromorphic function. It therefore must have a pole at some point z_0 in the unit cell. At this point, ψ_a must have a zero. We can then construct additional wave functions in the flat band by writing

$$\psi_{\mathbf{k}}(\mathbf{r}) = \frac{\vartheta_1\left(\frac{z-z_0}{a_1} + \frac{\mathbf{k}\cdot(\omega\mathbf{a}_1 - \mathbf{a}_2)}{2\pi} \,\middle|\, \frac{a_2}{a_1}\right)}{\vartheta_1\left(\frac{z-z_0}{a_1} \,\middle|\, \frac{a_2}{a_1}\right)} e^{i(\mathbf{k}\cdot\mathbf{a}_1)(z/a_1)}\psi_a(\mathbf{r}), \qquad (\text{D5})$$

where $a_i = a_{i,x} + a_{i,y}$, with $\mathbf{a}_i$ being lattice vectors. Here $\vartheta_1(z|\tau)$ is the Jacobi theta function, defined by

$$\vartheta_1(z|\tau) = \sum_{n=-\infty}^{\infty} (-1)^{n-1/2} e^{i\pi(n+1/2)^2\tau} e^{2\pi i(n+1/2)z}$$

$$= 2\sum_{n=0}^{\infty} (-1)^n e^{i\pi(n+1/2)^2\tau} \sin\left[2\pi(n+1/2)z\right]. \qquad (\text{D6})$$

Importantly, the pole of the ϑ_1 cancels the zero at ψ_a making $\psi_{\mathbf{k}}$ as defined above normalizable.

One can follow an alternative approach for the construction of the flat-band wave functions, which makes the similarity between the flat-band wave functions and the lowest Landau levels manifest. We can choose a basis of such functions in the form [42]

$$\psi(\mathbf{r}) = f(z)e^{-(\pi/2A)|z|^2}G(\mathbf{r}), \qquad (\text{D7})$$

where $f(z)$ is any holomorphic function, A is the unit cell area, and $G(\mathbf{r})$ is a structure function that captures the lattice dependency of the wave function. It is given by

$$G(\mathbf{r}) = \frac{e^{[\pi/2\operatorname{Im}(a_2/a_1)]\{|z/a_1|^2 + [z/a_1 - 2i\operatorname{Im}(z_0/a1)^2]\}}}{\vartheta_1\left(\frac{z-z_0}{a_1} \,\middle|\, \frac{a_2}{a_1}\right)} \psi_a(\mathbf{r}). \qquad (\text{D8})$$

Interestingly, it can be checked that $|G(\mathbf{r})|$ is periodic with the lattice.

APPENDIX E: C_3 SYMMETRY BREAKING IN CTBG

Here we discuss the effects of C_3 symmetry breaking in CTBG. For concreteness, we consider the Hamiltonian Eq. (D1) with

$$\mathcal{D} = \begin{pmatrix} -2ik_\theta^{-1}\bar{\partial} & \alpha U(\mathbf{r}) \\ \alpha U(-\mathbf{r}) & -2ik_\theta^{-1}\bar{\partial} \end{pmatrix},$$
$$U(\mathbf{r}) = (1+\beta)e^{-i\mathbf{q}_1\cdot\mathbf{r}} + e^{i\phi}e^{-i\mathbf{q}_2\cdot\mathbf{r}} + e^{-i\phi}e^{-i\mathbf{q}_3\cdot\mathbf{r}}, \qquad (\text{E1})$$

where $\mathbf{q}_1 = k_\theta(0, -1)$, $\mathbf{q}_{2,3} = k_\theta(\pm\sqrt{3}/2, 1/2)$, and $\phi = 2\pi/3$. Here α is the layer coupling scale and $\beta \ll 1$ is the C_3 symmetry-breaking scale.

Since the Hamiltonian still has a chiral and a reflection symmetry, each of v_x, v_y vanish with codimension one (as can be read from Table II). We also see that $\delta_Z = 1$, since besides the symmetry requirements, we have the additional relation between the chiral symmetry and the velocity operators, given by

$$v_y = -iSv_x$$
$$\Rightarrow \rho(v_y) = -i\rho(S)\rho(v_x), \qquad (\text{E2})$$

so $\rho(v_y) = 0$ if and only if $\rho(v_x) = 0$. This analysis shows us that the Dirac velocity can be tuned to vanish by tuning α even when C_3 is broken. On the other hand, for $\beta \neq 0$ the vanishing of the Dirac velocity is not accompanied by the exact vanishing of the band dispersion. Rather, the minimal bandwidth scales linearly with β at small β. The key insight for explaining the nonvanishing of the bandwidth is to note that the analysis presented in Appendix D requires the existence of two orthogonal zero-velocity wave functions $\psi_{a,b}$ in Eq. (D4) for which $\mathcal{I}(\mathbf{r}) = 0$. Here, $\mathcal{I}$ tends to zero, but $\psi_{a,b}$ become identical to one another.

When the C_3 symmetry is broken, the Dirac points are no longer fixed to the K, K' points. In fact, to the first order in β the displacement $\delta\mathbf{k}_D$ of the Dirac cones away from K, K' scales as $\delta\mathbf{k}_D = \mathcal{O}[\beta/v_D(\alpha)]$ and, therefore, *diverges* near the magic angle [75,76]. As a result of this divergence, when α is varied around the magic angle the Dirac cones travel around the BZ, meeting to form quadratic band-touching points (see Fig. 10). While the velocity (and hence $\mathcal{I}$) indeed vanishes at the QBT point, as required from our analysis of δ_Z, it only happens since ψ_a and ψ_b become identical to one another. When the Dirac cones form a QBT there is only a single zero-velocity $\sigma_z = 1$ wave function at this point. In that case, $\nu(\mathbf{r})$ as defined in Eq. (D4) is
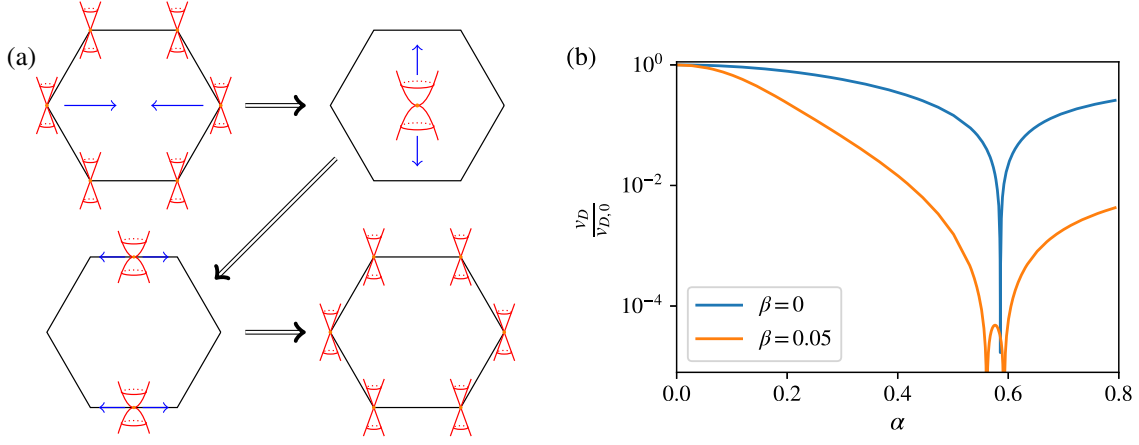
FIG. 10. (a) The trajectory of the Dirac points in a C_3-broken CTBG near the magic angle when α is varied. For a small symmetry-breaking parameter β the Dirac cones remain close to the K, K' points away from the magic angle. Near the magic angle, the displacement δk_D diverges and the Dirac cones travel around the BZ, meeting twice to form QBT points at the Γ and M points. (b) The normalized Dirac velocity at the Dirac cones for C_3-symmetric ($\beta = 0$) and weakly C_3-broken ($\beta = 0.05$) CTBG Hamiltonian Eq. (E1). In the C_3-broken case, the Dirac velocity vanishes twice, at the two QBT points.

constant, does not have any poles, and therefore does not guarantee any zeros of ψ_a.

APPENDIX F: C_4 SYMMETRY BREAKING IN THE C4FB MODEL

The C4FB model Eq. (45) gives a subtle example to our analysis of δ_Z and in particular the theorem we prove in Appendix A. To simplify our analysis, we begin by constructing a continuum model with the same symmetries as the C4FB model, but which is easier to analyze. We consider

$$\mathcal{H} = \boldsymbol{k} \cdot \boldsymbol{\sigma} + \alpha T(\boldsymbol{r}), \tag{F1}$$

$$T(\boldsymbol{r}) = \eta_y \sum_n [1 + (-1)^n \beta_1] e^{i \boldsymbol{q}_n \cdot \boldsymbol{r}} [\cos(\theta_n)\sigma_x + \sin(\theta_n)\sigma_y]$$
$$+ \eta_x \sum_n [1 + (-1)^n \beta_2] e^{i \boldsymbol{q}'_n \cdot \boldsymbol{r}} [\cos(\theta'_n)\sigma_x + \sin(\theta'_n)\sigma_y],$$
$$\tag{F2}$$

where $\theta_n = \{0, (\pi/2), \pi, (3\pi/2)\}$, $\theta'_n = \{(\pi/4), (3\pi/4), (5\pi/4), (7\pi/4)\}$, and the inverse lattice vectors are given by $\boldsymbol{q}_n = (\cos\theta_n, \sin\theta_n)$, $\boldsymbol{q}'_n = (\cos\theta'_n, \sin\theta'_n)$ (see Fig. 11). The Hamiltonian has four degenerate zero-energy wave functions at $\boldsymbol{k} = 0$, corresponding to two copies of the Dirac cone.

The terms $\beta_{1,2}$ break the C_4 symmetry of the model to C_2. Note that when either of $\beta_{1,2}$ is zero there remains a reflection symmetry. From Table III we see that in the presence of any reflection symmetry we have $\delta_Z = 1$. In the discussion of the C_4-symmetric model, we show that when the model has flat bands there must be at least 8 flat bands at $E = 0$ (4 per S eigenvalue). A similar argument shows

that in the presence of a weaker C_2 symmetry we must have at least 4 flat bands (2 per S eigenvalue).

Interestingly, we find [Fig. 12(a)] that the magic angle obtained by tuning α at $\beta_{1,2} = 0$ is unstable when the C_4 symmetry is broken by a nonzero $\beta_{1,2}$. That is, taking $\beta_2 = 0$, $\beta_1 \neq 0$, for example, the codimension of the zero Dirac velocity manifold in the (α, β_1) space is not $\delta_Z = 1$ as can naively be expected from Table III. Rather, the velocity vanishes on a point in (α, β_1) space (where $\beta_1 = 0$).

This apparent contradiction is resolved by noting that once either β_1 or β_2 is nonzero, the conditions of the theorem we prove in Appendix A are not satisfied, and Table III cannot be used to infer the codimension. Namely, the theorem requires that there is a gap between the Dirac cone and the higher bands. In the case discussed here, for $\beta_{1,2} = 0$ the C_4 symmetry requires that there are 8 degenerate zero-energy bands at the magic angle. Since the Dirac cone is only fourfold degenerate, there must be 4 additional states closing the band gap (see Fig. 13). In the presence of the C_4 symmetry the additional bands do not hybridize with the Dirac point wave functions as they have different C_4
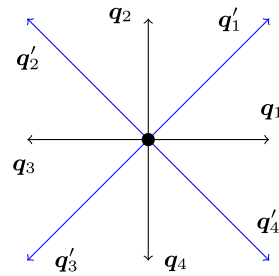

FIG. 11. Tunneling vectors for the simplified C4FB model Eq. (F2). The blue and black vectors correspond to the terms in the first and second row of Eq. (F2), respectively.
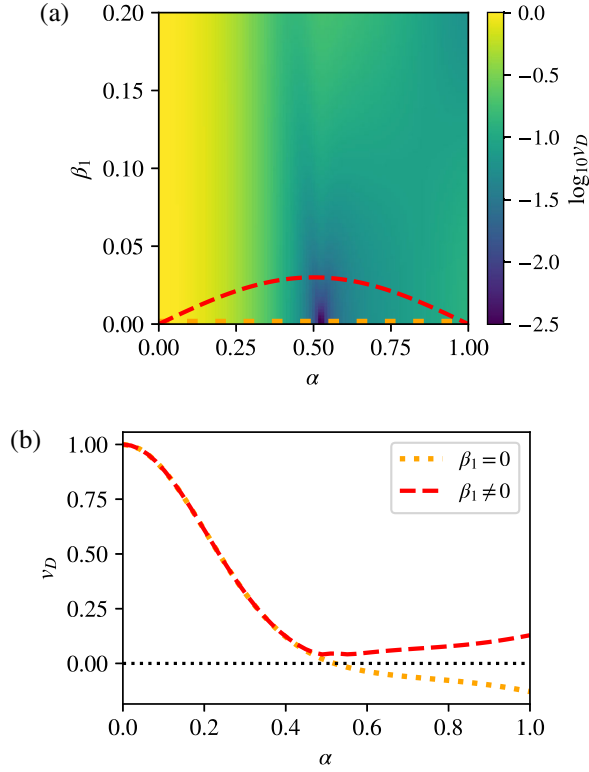
FIG. 12. (a) The value of the Dirac velocity at the Dirac cone for the Hamiltonian Eq. (F2) with a broken C_4 symmetry. The codimension of the zero Dirac velocity manifold is two (the dark point). (b) The values of the "signed" Dirac velocity f [as defined in Eq. (5)] going through two different trajectories. Since the wave functions are discontinuous at the magic angle, the velocities acquire an opposite sign.

eigenvalues, and we can still use the results of Appendix A. On the other hand, C_4 breaking couples the Dirac cones and higher-band wave functions, breaking the assumptions made in the theorem.
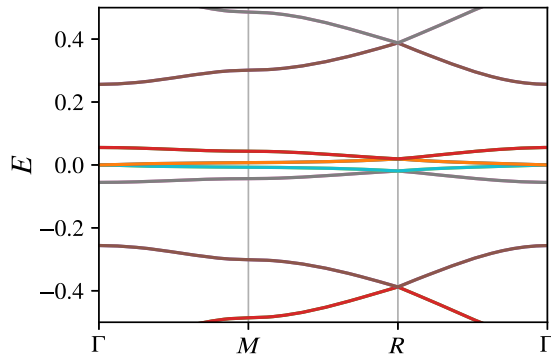

FIG. 13. The band structure of the C4FB model near the parameter values at which the velocity vanishes. Each band in the picture is doubly degenerate as a result of an antiunitary symmetry $C_2 T'$ that squares to -1. We therefore find that there are eight bands connected to $E = 0$, all of which become exactly flat when the velocity vanishes.

A different way of understanding this phenomenon is that the definition of f as in Eq. (5) is by adiabatic continuation: we always require that the wave functions are changed continuously as we vary the control parameters. Since the Dirac points wave functions are changed discontinuously at the magic angle, f cannot be defined to be both continuous and single valued. As an example, in Fig. 12(b) we draw $f(\alpha, \beta_1)$ going in two trajectories, one with $\beta_1 = 0$ and the other with nonzero β_1. The sign obtained for $f(\alpha, \beta_1)$ is opposite as a result of the discontinuity.

APPENDIX G: PERTURBATION THEORY FOR THE C_n-SYMMETRIC QUASICRYSTALLINE MODELS

Here we calculate in perturbation theory the formal Dirac velocity for the quasicrystalline models Eq. (59).

1. Perturbation theory: Analytical results

Let us calculate the first orders for the perturbation series giving v_D. The wave functions are given in the form

$$\psi_K(\mathbf{r}) = \frac{1}{N} \begin{pmatrix} \psi_0(\mathbf{r}) + \alpha^2 \psi_2(\mathbf{r}) + \cdots \\ \alpha \psi_1(\mathbf{r}) + \cdots \end{pmatrix}, \qquad \text{(G1)}$$

where N is a normalization constant. ψ_i are obtained from Eq. (60). The first terms are given by

TABLE II. δ_Z for a single Dirac cone. The codimension δ_Z of the zero Dirac velocity manifold for a single nondegenerate Dirac cone, according to the symmetry group, with the symmetries Θ, Π, Σ, R defined in Eq. (6). In the column of each symmetry a zero denotes the absence of the symmetry, while the sign denotes the square of the symmetry. The signs of the reflection operator $R_{\zeta_\Theta, \zeta_\Pi}$ reflect the commutation relations of R with Θ, Π. We omit the rows that could not give rise to a single Dirac cone with the listed symmetries. Center dots signify symmetry groups which cannot support the algebra of a Dirac cone. For each symmetry group we specify a representation for the Θ, Π, Σ, R operators and write matrices spanning the linear space of possible v_x representations that satisfy Eqs. (6) and (7). δ_Z is then the dimension of this linear space.

Θ	Π	Σ	R	$\rho(\Theta)$	$\rho(\Pi)$	$\rho(\Sigma)$	$\rho(R)$	$\rho(v_x)$	δ_Z
0	0	0	R	$\cdots$	$\cdots$	$\cdots$	σ_y	$\sigma_{x,z}$	2
			0	$\cdots$	$\cdots$	$\cdots$	$\cdots$	$\sigma_{x,y,z}$	3
0	0	1	R_-	$\cdots$	$\cdots$	σ_z	σ_y	σ_x	1
			0	$\cdots$	$\cdots$	σ_z	$\cdots$	$\sigma_{x,y}$	2
0	+	0	R_+	$\cdots$	$\sigma_x K$	$\cdots$	σ_y	σ_x	1
			0	$\cdots$	$\sigma_x K$	$\cdots$	$\cdots$	$\sigma_{x,y}$	2
$-$	+	0	R_{-+}	$\sigma_y K$	$\sigma_x K$	σ_z	σ_y	σ_x	1
			0	$\sigma_y K$	$\sigma_x K$	σ_z	$\cdots$	$\sigma_{x,y}$	2
$-$	0	0	R_-	$\sigma_y K$	$\cdots$	$\cdots$	σ_y	$\sigma_{x,z}$	2
			0	$\sigma_y K$	$\cdots$	$\cdots$	$\cdots$	$\sigma_{x,y,z}$	3

TABLE III. δ_Z for two degenerate Dirac cones: Same as Table II but for doubly degenerate Dirac cones. Center dots in the δ_Z column signify symmetry groups which cannot support the algebra of a Dirac cone.

Θ	Π	Σ	R	$\rho(\Theta)$	$\rho(\Pi)$	$\rho(\Sigma)$	$\rho(R)$	$\rho(v_x)$	δ_Z
0	0	0	R	$\cdots$	$\cdots$	$\cdots$	σ_y	$\sigma_{x,z}, \sigma_{x,z}\eta_{x,y,z}$	8
			0	$\cdots$	$\cdots$	$\cdots$	$\cdots$	$\sigma_{x,y,z}, \eta_{x,y,z}, \sigma_{x,y,z}\eta_{x,y,z}$	15
0	0	1	R_-	$\cdots$	$\cdots$	σ_z	σ_y	$\sigma_x, \eta_{x,y,z}\sigma_x$	4
			R_+	$\cdots$	$\cdots$	η_z	σ_y	$\sigma_{x,z}\eta_{x,y}$	4
			0	$\cdots$	$\cdots$	σ_z	$\cdots$	$\sigma_{x,y}, \sigma_{x,y}\eta_{x,y,z}$	8
+	0	0	R_+	$\eta_y\sigma_y K$	$\cdots$	$\cdots$	$\eta_y\sigma_y$	$\sigma_{x,z}, \eta_{x,z}$	4
			R_-	$\eta_y\sigma_y K$	$\cdots$	$\cdots$	σ_y	$\sigma_{x,z}$	2
			0	$\eta_y\sigma_y K$	$\cdots$	$\cdots$	$\cdots$	$\sigma_{x,y,z}, \eta_{x,y,z}$	6
+	+	1	R_{++}	$\eta_y\sigma_y K$	$\sigma_x K$	$\eta_y\sigma_z$	$\eta_x\sigma_y$	σ_x, η_y	2
			R_{--}	$\cdots$	$\cdots$	$\cdots$	$\cdots$	$\cdots$	$\cdots$
			R_{+-}	$\eta_y\sigma_y K$	$\sigma_x K$	$\eta_y\sigma_z$	$\eta_y\sigma_y$	$\sigma_x, \eta_{x,z}$	3
			R_{-+}	$\eta_y\sigma_y K$	$\sigma_x K$	$\eta_y\sigma_z$	σ_y	σ_x	1
			0	$\eta_y\sigma_y K$	$\sigma_x K$	$\cdots$	$\cdots$	$\sigma_{x,y}, \eta_{x,z}$	4
0	+	0	R_+	$\cdots$	$\sigma_x K$	$\cdots$	σ_y	$\sigma_x, \sigma_z\eta_y, \sigma_x\eta_{x,z}$	4
			R_-	$\cdots$	$\sigma_x K$	$\cdots$	$\eta_y\ \sigma_y$	$\sigma_x, \sigma_y\eta_{x,z}, \eta_{x,z}, \eta_y\sigma_z$	7
			0	$\cdots$	$\sigma_x K$	$\cdots$	$\cdots$	$\sigma_{x,y}, \sigma_z\eta_y, \eta_{z,x}, \sigma_{x,y}\eta_{z,x}$	9
−	+	1	R_{++}	$\eta_z\sigma_y K$	$\sigma_x K$	$\sigma_z\eta_z$	$\eta_x\sigma_y$	$\sigma_x, \sigma_y\eta_z$	2
			R_{--}	$\eta_z\sigma_y K$	$\sigma_x K$	$\sigma_z\eta_z$	$\eta_y\sigma_y$	$\sigma_x, \eta_x, \eta_z\sigma_y, \eta_y\sigma_z$	4
			R_{+-}	$\sigma_y K$	$\sigma_x K$	σ_z	$\eta_y\sigma_y$	$\sigma_x, \sigma_y\eta_{x,z}$	3
			R_{-+}	$\sigma_y K$	$\sigma_x K$	σ_z	σ_y	$\sigma_x, \sigma_x\eta_{x,z}$	3
			0	$\sigma_y K$	$\sigma_x K$	σ_z	$\cdots$	$\sigma_{x,y}, \sigma_{x,y}\eta_{x,z}$	6
−	0	0	R_+	$\sigma_y K$	$\cdots$	$\cdots$	$\eta_y\sigma_y$	$\sigma_{x,z}, \sigma_y\eta_{x,z}, \eta_y$	5
			R_-	$\sigma_y K$	$\cdots$	$\cdots$	σ_y	$\sigma_{x,z}, \sigma_{x,z}\eta_{x,z}$	6
			0	$\sigma_y K$	$\cdots$	$\cdots$	$\cdots$	$\sigma_{x,y,z}, \sigma_{x,y,z}\eta_{x,z}, \eta_y$	10
−	−	1	R_{++}	$\cdots$	$\cdots$	$\cdots$	$\cdots$	$\cdots$	$\cdots$
			R_{--}	$\eta_x\sigma_y K$	$\eta_y\sigma_x K$	$\sigma_z\eta_z$	$\eta_y\sigma_y$	$\sigma_x, \sigma_z\eta_y$	2
			R_{+-}	$\sigma_y K$	$\eta_y\sigma_x K$	$\sigma_z\eta_y$	$\eta_y\sigma_y$	σ_x	1
			R_{-+}	$\sigma_y K$	$\eta_y\sigma_x K$	$\sigma_z\eta_y$	σ_y	$\sigma_x, \sigma_z\eta_{x,z}$	3
			0	$\eta_x\sigma_y K$	$\eta_y\sigma_x K$	$\sigma_z\eta_z$	$\cdots$	$\sigma_{x,y}, \sigma_z\eta_{x,y}$	4
0	−	0	R_+	$\cdots$	$\eta_y\sigma_x K$	$\cdots$	σ_y	$\sigma_x, \sigma_z\eta_{x,y,z}$	4
			R_-	$\cdots$	$\eta_y\sigma_x K$	$\cdots$	$\eta_y\sigma_y$	$\sigma_x, \sigma_z\eta_y$	2
			0	$\cdots$	$\eta_y\sigma_x K$	$\cdots$	$\cdots$	$\sigma_{x,y}, \sigma_z\eta_{x,y,z}$	5
+	−	1	R_{++}	$\cdots$	$\cdots$	$\cdots$	$\cdots$	$\cdots$	$\cdots$
			R_{--}	$\cdots$	$\cdots$	$\cdots$	$\cdots$	$\cdots$	$\cdots$
			R_{+-}	$\eta_y\sigma_y K$	$\eta_y\sigma_x K$	σ_z	$\eta_y\sigma_y$	σ_x	1
			R_{-+}	$\eta_y\sigma_y K$	$\eta_y\sigma_x K$	σ_z	σ_y	σ_x	1
			0	$\eta_y\sigma_y K$	$\eta_y\sigma_x K$	σ_z	$\cdots$	$\sigma_{x,y}$	2

$$\psi_0(\mathbf{r}) = 1,$$

$$\psi_1(\mathbf{r}) = -i\sum_{j=1}^{n} e^{i\mathbf{q}_j\cdot\mathbf{r}},$$

$$\psi_2(\mathbf{r}) = -\sum_{k=1}^{n-1}\sum_{j=0}^{n-1} \frac{e^{-i(\mathbf{q}_{j+k}-\mathbf{q}_j)\cdot\mathbf{r}}}{1-e^{i(2\pi p/n)k}},$$

$$\psi_3(\mathbf{r}) = i\sum_{l=0}^{n-1}\sum_{k=1}^{n-1}\sum_{j=1}^{n-1}$$

$$\times \frac{e^{-i(\mathbf{q}_{j+k}-\mathbf{q}_j-\mathbf{q}_{j+k+l})\cdot\mathbf{r}}}{(1-e^{i(2\pi/n)k})(1+e^{-(2\pi i/n)(k+l)}-e^{(2\pi i/n)l})}. \quad \text{(G2)}$$

The velocities are then obtained using Eq. (61) and are given in the form

$$v_D = \frac{1 + v_2\alpha^2 + v_4\alpha^4 + \cdots}{1 + N_2\alpha^2 + N_4\alpha^4 + \cdots} \cdot v_0, \quad \text{(G3)}$$

with the first coefficients given by

$$v_2 = -n, \quad \text{(G4)}$$

$$v_4 = n\sum_{k=1}^{n-1}\left[\frac{1 - 2\cos\frac{2\pi k}{n} + \cos\frac{4\pi k}{n}}{16\sin^4\frac{\pi k}{n}} - \frac{\cos\frac{2\pi k}{n} - \cos\frac{4\pi k}{n}}{2\sin^2\frac{\pi k}{n}}\right], \quad \text{(G5)}$$

$$N_2 = n, \tag{G6}$$

$$N_4 = n \sum_{k=1}^{n-1} \frac{1 + 2\cos\frac{2\pi k}{n} - 2\cos\frac{4\pi k}{n}}{4\sin^2\frac{\pi k}{n}}. \tag{G7}$$

By solving for $v_D = 0$ we can calculate the first magic angle for any n. Importantly, since $\delta_Z = 1$, the coefficients of the perturbation expansion are real, which allows us to find a magic angle at finite α.

2. Perturbation theory: Numerical results

We can numerically calculate higher orders in the perturbation series for $n = 5$. We find

$$v_D(n=5) = v_0$$
$$\times \frac{1 - 5\alpha^2 - 10\alpha^4 - 177.6\alpha^6 - 1105.5\alpha^8 - 9309.2\alpha^{10} + \cdots}{1 + 5\alpha^2 + 20\alpha^4 + 115.2\alpha^6 + 1705.0\alpha^8 + 18841.0\alpha^{10} + \cdots}, \tag{G8}$$

which gives a magic angle at $\alpha_0 = 0.32$.

---

[1] R. Bistritzer and A. H. MacDonald, *Moiré Bands in Twisted Double-Layer Graphene*, Proc. Natl. Acad. Sci. U.S.A. **108**, 12233 (2011).

[2] E. Suárez Morell, J. D. Correa, P. Vargas, M. Pacheco, and Z. Barticevic, *Flat Bands in Slightly Twisted Bilayer Graphene: Tight-Binding Calculations*, Phys. Rev. B **82**, 121407(R) (2010).

[3] Y. Cao, V. Fatemi, S. Fang, K. Watanabe, T. Taniguchi, E. Kaxiras, and P. Jarillo-Herrero, *Unconventional Superconductivity in Magic-Angle Graphene Superlattices*, Nature (London) **556**, 43 (2018).

[4] Y. Cao, V. Fatemi, A. Demir, S. Fang, S. L. Tomarken, J. Y. Luo, J. D. Sanchez-Yamagishi, K. Watanabe, T. Taniguchi, E. Kaxiras, R. C. Ashoori, and P. Jarillo-Herrero, *Correlated Insulator Behaviour at Half-Filling in Magic-Angle Graphene Superlattices*, Nature (London) **556**, 80 (2018).

[5] E. Khalaf, A. J. Kruchkov, G. Tarnopolsky, and A. Vishwanath, *Magic Angle Hierarchy in Twisted Graphene Multilayers*, Phys. Rev. B **100**, 085109 (2019).

[6] S. Carr, C. Li, Z. Zhu, E. Kaxiras, S. Sachdev, and A. Kruchkov, *Ultraheavy and Ultrarelativistic Dirac Quasiparticles in Sandwiched Graphenes*, Nano Lett. **20**, 3030 (2020).

[7] Z. Zhu, S. Carr, D. Massatt, M. Luskin, and E. Kaxiras, *Twisted Trilayer Graphene: A Precisely Tunable Platform for Correlated Electrons*, Phys. Rev. Lett. **125**, 116404 (2020).

[8] J. M. Park, Y. Cao, K. Watanabe, T. Taniguchi, and P. Jarillo-Herrero, *Tunable Strongly Coupled Superconductivity in Magic-Angle Twisted Trilayer Graphene*, Nature (London) **590**, 249 (2021).

[9] P. A. Volkov, J. H. Wilson, and J. Pixley, *Magic Angles and Correlations in Twisted Nodal Superconductors*, arXiv:2012.07860.

[10] O. Can, T. Tummuru, R. P. Day, I. Elfimov, A. Damascelli, and M. Franz, *High-Temperature Topological Superconductivity in Twisted Double-Layer Copper Oxides*, Nat. Phys. **17**, 519 (2021).

[11] J. Cano, S. Fang, J. H. Pixley, and J. H. Wilson, *Moiré Superlattice on the Surface of a Topological Insulator*, Phys. Rev. B **103**, 155157 (2021).

[12] T. Wang, N. F. Q. Yuan, and L. Fu, *Moiré Surface States and Enhanced Superconductivity in Topological Insulators*, Phys. Rev. X **11**, 021024 (2021).

[13] A. Dunbrack and J. Cano, *Magic Angle Conditions for Twisted 3D Topological Insulators*, Phys. Rev. B **106**, 075142 (2022).

[14] D. Xiao, M.-c. Chang, and Q. Niu, *Berry Phase Effects on Electronic Properties*, Rev. Mod. Phys. **82**, 1959 (2010).

[15] G. Tarnopolsky, A. J. Kruchkov, and A. Vishwanath, *Origin of Magic Angles in Twisted Bilayer Graphene*, Phys. Rev. Lett. **122**, 106405 (2019).

[16] S. Becker, M. Embree, J. Wittsten, and M. Zworski, *Spectral Characterization of Magic Angles in Twisted Bilayer Graphene*, Phys. Rev. B **103**, 165113 (2021).

[17] F. K. Popov and A. Milekhin, *Hidden Wave Function of Twisted Bilayer Graphene: The Flat Band as a Landau Level*, Phys. Rev. B **103**, 155150 (2021).

[18] A. Altland and M. R. Zirnbauer, *Nonstandard Symmetry Classes in Mesoscopic Normal-Superconducting Hybrid Structures*, Phys. Rev. B **55**, 1142 (1997).

[19] M.-R. Li, A.-L. He, and H. Yao, *Magic-Angle Twisted Bilayer Systems with Quadratic Band Touching: Exactly Flat Bands with High Chern Number*, Phys. Rev. Res. **4**, 043151 (2022).

[20] G. W. Moore, *Quantum Symmetries and Compatible Hamiltonians*, http://www.physics.rutgers.edu/gmoore/QuantumSymmetryBook.pdf.

[21] T. Morimoto and A. Furusaki, *Topological Classification with Additional Symmetries from Clifford Algebras*, Phys. Rev. B **88**, 125129 (2013).

[22] C.-K. Chiu, H. Yao, and S. Ryu, *Classification of Topological Insulators and Superconductors in the Presence of Reflection Symmetry*, Phys. Rev. B **88**, 075142 (2013).

[23] C.-K. Chiu, J. C. Y. Teo, A. P. Schnyder, and S. Ryu, *Classification of Topological Quantum Matter with Symmetries*, Rev. Mod. Phys. **88**, 035005 (2016).

[24] N. P. Armitage, E. J. Mele, and A. Vishwanath, *Weyl and Dirac Semimetals in Three-Dimensional Solids*, Rev. Mod. Phys. **90**, 015001 (2018).

[25] Z. Song, Z. Wang, W. Shi, G. Li, C. Fang, and B. A. Bernevig, *All Magic Angles in Twisted Bilayer Graphene Are Topological*, Phys. Rev. Lett. **123**, 036401 (2019).

[26] M. G. Scheer, K. Gu, and B. Lian, *Magic Angles in Twisted Bilayer Graphene near Commensuration: Towards a Hypermagic Regime*, Phys. Rev. B **106**, 115418 (2022)

[27] Note that spinful reflection symmetry is given by $M_x = \sigma_x(x \to -x)$. Here we choose a gauge in which the Dirac-cone Hamiltonian is of the form $\boldsymbol{k} \cdot \boldsymbol{\sigma}$ which gives the present definition of M_x.

[28] M. Katsnelson, K. Novoselov, and A. Geim, *Chiral Tunnelling and the Klein Paradox in Graphene*, Nat. Phys. **2,** 620 (2006).

[29] X. Wen, *Metallic Non-Fermi-Liquid Fixed Point in Two and Higher Dimensions*, Phys. Rev. B **42,** 6623 (1990).

[30] T. Giamarchi, *Quantum Physics in One Dimension*, Vol. 121 (Clarendon Press, Oxford, 2003).

[31] P. Wang, G. Yu, Y. H. Kwan, Y. Jia, S. Lei, S. Klemenz, F. A. Cevallos, T. Devakul, K. Watanabe, T. Taniguchi *et al.*, *One-Dimensional Luttinger Liquids in a Two-Dimensional Moiré Lattice*, Nature (London) **605,** 57 (2022).

[32] N. F. Yuan, H. Isobe, and L. Fu, *Magic of High-Order van Hove Singularity*, Nat. Commun. **10,** 1 (2019).

[33] N. F. Q. Yuan and L. Fu, *Classification of Critical Points in Energy Bands Based on Topology, Scaling, and Symmetry*, Phys. Rev. B **101,** 125120 (2020).

[34] C. Forsythe, X. Zhou, K. Watanabe, T. Taniguchi, A. Pasupathy, P. Moon, M. Koshino, P. Kim, and C. R. Dean, *Band Structure Engineering of 2D Materials Using Patterned Dielectric Superlattices*, Nat. Nanotechnol. **13,** 566 (2018).

[35] R. L. Willett, M. A. Paalanen, R. R. Ruel, K. W. West, L. N. Pfeiffer, and D. J. Bishop, *Anomalous Sound Propagation at $\nu = 1/2$ in a 2D Electron Gas: Observation of a Spontaneously Broken Translational Symmetry?*, Phys. Rev. Lett. **65,** 112 (1990).

[36] S. H. Simon, *Coupling of Surface Acoustic Waves to a Two-Dimensional Electron Gas*, Phys. Rev. B **54,** 13878 (1996).

[37] N. Bultinck, E. Khalaf, S. Liu, S. Chatterjee, A. Vishwanath, and M. P. Zaletel, *Ground State and Hidden Symmetry of Magic-Angle Graphene at Even Integer Filling*, Phys. Rev. X **10,** 031034 (2020).

[38] P. San-Jose, J. González, and F. Guinea, *Non-Abelian Gauge Potentials in Graphene Bilayers*, Phys. Rev. Lett. **108,** 216802 (2012).

[39] A. P. Schnyder, S. Ryu, A. Furusaki, and A. W. W. Ludwig, *Classification of Topological Insulators and Superconductors in Three Spatial Dimensions*, Phys. Rev. B **78,** 195125 (2008).

[40] A. P. Schnyder, S. Ryu, and A. W. W. Ludwig, *Lattice Model of a Three-Dimensional Topological Singlet Superconductor with Time-Reversal Symmetry*, Phys. Rev. Lett. **102,** 196804 (2009).

[41] J. Wang, J. Cano, A. J. Millis, Z. Liu, and B. Yang, *Exact Landau Level Description of Geometry and Interaction in a Flatband*, Phys. Rev. Lett. **127,** 246403 (2021).

[42] Y. Sheffer and A. Stern, *Chiral Magic-Angle Twisted Bilayer Graphene in a Magnetic Field: Landau Level Correspondence, Exact Wave Functions, and Fractional Chern Insulators*, Phys. Rev. B **104,** 124105 (2021).

[43] The transition at one flux quantum in magic-angle CTBG in a magnetic field [17,42] can be seen as a transition from a $(1, -1)$ index to $(2, 0)$.

[44] J. Wang, Y. Zheng, A. J. Millis, and J. Cano, *Chiral Approximation to Twisted Bilayer Graphene: Exact Intravalley Inversion Symmetry, Nodal Structure, and Implications for Higher Magic Angles*, Phys. Rev. Res. **3,** 023155 (2021).

[45] B. Sutherland, *Localization of Electronic Wave Functions due to Local Topology*, Phys. Rev. B **34,** 5208 (1986).

[46] D. L. Bergman, C. Wu, and L. Balents, *Band Touching from Real-Space Topology in Frustrated Hopping Models*, Phys. Rev. B **78,** 125104 (2008).

[47] Y. Hwang, J.-W. Rhim, and B.-J. Yang, *General Construction of Flat Bands with and without Band Crossings Based on Wave Function Singularity*, Phys. Rev. B **104,** 085144 (2021).

[48] D. Călugăru, A. Chew, L. Elcoro, Y. Xu, N. Regnault, Z.-D. Song, and B. A. Bernevig, *General Construction and Topological Classification of Crystalline Flat Bands*, Nat. Phys. **18,** 185 (2022).

[49] A. J. Kollár, M. Fitzpatrick, P. Sarnak, and A. A. Houck, *Line-Graph Lattices: Euclidean and Non-Euclidean Flat Bands, and Implementations in Circuit Quantum Electrodynamics*, Commun. Math. Phys. **376,** 1909 (2020).

[50] C. S. Chiu, D.-S. Ma, Z.-D. Song, B. A. Bernevig, and A. A. Houck, *Fragile Topology in Line-Graph Lattices with Two, Three, or Four Gapped Flat Bands*, Phys. Rev. Res. **2,** 043414 (2020).

[51] C.-M. Jian, Z.-C. Gu, and X.-L. Qi, *Momentum-Space Instantons and Maximally Localized Flat-Band Topological Hamiltonians*, Phys. Status Solidi RRL **7,** 154 (2013).

[52] L. Chen, T. Mazaheri, A. Seidel, and X. Tang, *The Impossibility of Exactly Flat Non-Trivial Chern Bands in Strictly Local Periodic Tight Binding Models*, J. Phys. A **47,** 152001 (2014).

[53] G. Chaudhary, A. A. Burkov, and O. G. Heinonen, *Twisted Bilayers of Thin Film Magnetic Topological Insulators*, Phys. Rev. Res. **4,** 043034 (2022).

[54] L. Fu, C. L. Kane, and E. J. Mele, *Topological Insulators in Three Dimensions*, Phys. Rev. Lett. **98,** 106803 (2007).

[55] J. E. Moore and L. Balents, *Topological Invariants of Time-Reversal-Invariant Band Structures*, Phys. Rev. B **75,** 121306(R) (2007).

[56] R. Roy, *Topological Phases and the Quantum Spin Hall Effect in Three Dimensions*, Phys. Rev. B **79,** 195322 (2009).

[57] M. Z. Hasan and C. L. Kane, *Colloquium: Topological Insulators*, Rev. Mod. Phys. **82,** 3045 (2010).

[58] A similar argument can be used in the CTBG Hamiltonian Eq. (B5) to find that there must be at least three zeros per unit cell for the translation symmetry of the model. Notice, however, that the Hamiltonian presented in the gauge choice of Eq. (B5) has a unit cell which is 3 times larger than the physical unit cell.

[59] P. J. Ledwith, G. Tarnopolsky, E. Khalaf, and A. Vishwanath, *Fractional Chern Insulator States in Twisted Bilayer Graphene: An Analytical Approach*, Phys. Rev. Res. **2,** 023237 (2020).

[60] E. T. Whittaker and G. N. Watson, *A Course of Modern Analysis* (Cambridge University Press, Cambridge, England, 1996).

[61] F. D. M. Haldane and E. H. Rezayi, *Periodic Laughlin-Jastrow Wave Functions for the Fractional Quantized Hall Effect*, Phys. Rev. B **31,** 2529 (1985).

[62] J. Wang and Z. Liu, *Hierarchy of Ideal Flatbands in Chiral Twisted Multilayer Graphene Models*, Phys. Rev. Lett. **128,** 176403 (2022).

[63] P. J. Ledwith, A. Vishwanath, and E. Khalaf, *Family of Ideal Chern Flatbands with Arbitrary Chern Number in Chiral*

Twisted Graphene Multilayers, Phys. Rev. Lett. **128,** 176404 (2022).

[64] D. Guerci, J. Wang, J. Pixley, and J. Cano, *Designer Meron Lattice on the Surface of a Topological Insulator*, Phys. Rev. B **106,** 245417 (2022).

[65] M. Levin, F. J. Burnell, M. Koch-Janusz, and A. Stern, *Exactly Soluble Models for Fractional Topological Insulators in Two and Three Dimensions*, Phys. Rev. B **84,** 235145 (2011).

[66] P. Bonderson, C. Nayak, and X.-L. Qi, *A Time-Reversal Invariant Topological Phase at the Surface of a 3D Topological Insulator*, J. Stat. Mech. (2013) P09016.

[67] C. Wang, A. C. Potter, and T. Senthil, *Gapped Symmetry Preserving Surface State for the Electron Topological Insulator*, Phys. Rev. B **88,** 115137 (2013).

[68] X. Chen, L. Fidkowski, and A. Vishwanath, *Symmetry Enforced Non-Abelian Topological Order at the Surface of a Topological Insulator*, Phys. Rev. B **89,** 165132 (2014).

[69] M. A. Metlitski, C. L. Kane, and M. P. A. Fisher, *Symmetry-Respecting Topologically Ordered Surface Phase of Three-Dimensional Electron Topological Insulators*, Phys. Rev. B **92,** 125111 (2015).

[70] A. Stern, *Fractionalized Two-Dimensional States on Surfaces of Three Dimensional Topological Insulators*, Journal Club for Condensed Matter Physics, 10.36471/JCCM_October_2013_03 (2013).

[71] R. Bistritzer and A. H. MacDonald, *Moiré Butterflies in Twisted Bilayer Graphene*, Phys. Rev. B **84,** 035440 (2011).

[72] P. J. Ledwith, E. Khalaf, and A. Vishwanath, *Strong Coupling Theory of Magic-Angle Graphene: A Pedagogical Introduction*, Ann. Phys. (Amsterdam) **435,** 168646 (2021).

[73] N. N. T. Nam and M. Koshino, *Lattice Relaxation and Energy Band Modulation in Twisted Bilayer Graphene*, Phys. Rev. B **96,** 075311 (2017).

[74] H. C. Po, L. Zou, A. Vishwanath, and T. Senthil, *Origin of Mott Insulating Behavior and Superconductivity in Twisted Bilayer Graphene*, Phys. Rev. X **8,** 031089 (2018).

[75] Y. H. Kwan, S. A. Parameswaran, and S. L. Sondhi, *Twisted Bilayer Graphene in a Parallel Magnetic Field*, Phys. Rev. B **101,** 205116 (2020).

[76] O. Antebi, A. Stern, and E. Berg, *In-Plane Orbital Magnetization as a Probe for Symmetry Breaking in Strained Twisted Bilayer Graphene*, Phys. Rev. B **105,** 104423 (2022).